



MASTER THESIS

Title

“Effective theories for pseudogap metals”

Author

Julia Brunkert

Aspired Academic Degree

Master of Science – MSc

Munich; 06.08.2020

Universities: Ludwig-Maximilians-Universität München & Technische Universität München

Course: Theoretical and Mathematical Physics (TMP)

Supervisor: Prof. Dr. Matthias Punk

Abstract

Julia Brunkert¹

¹) Ludwig-Maximilians-Universität and TU München
jbrunkert@yahoo.de

The pseudogap phase, which occurs in high temperature superconductors, is an unconventional metallic phase with unusual properties. For example, it exhibits Fermi liquid like transport, but an anomalously low carrier density, which is not in accordance with Luttinger's theorem. Interestingly, a phase with similar properties has recently been found in twisted bilayer graphene, a material with a vastly different microscopic structure. In this thesis we will pursue two different strategies to model the behavior of these so-called pseudogap metals.

First, starting from an exactly solvable dimer model for the description of pseudogap metals we add a magnetic field and compute the corresponding energy spectrum. The so obtained Hofstadter butterfly plot gives a prediction of the magnetic response of magic angle twisted bilayer graphene.

Second, by developing a novel slave boson construction for the t-J model we will show that this description (at the saddle point) omits four different phases: Fermi liquid, superconducting phase and U(1) and \mathbb{Z}_2 fractionalized Fermi liquid. This slave boson description is able to describe the small Fermi surfaces of the pseudogap metal. Also in a certain parameter regime this description maps to the more general dimer model introduced in the beginning.

Acknowledgements

I would like to thank my supervisor Matthias Punk for his support, whenever I needed it, and also for his endless patience.

Furthermore, I want to thank my friends for their moral support. Their support, especially during the Corona time, was of great help. They helped me to procrastinate at many times, but enabled me to be productive at other times- at some point we even defined a complex measure for productivity.

Lastly, I want to thank my family for always being there for me even at 700 km distance.

Contents

1	Introduction	1
2	Dimers on the square and the triangular lattice	4
2.1	Bosonic Dimers	4
2.1.1	Introduction and naming	5
2.1.2	RK Hamiltonian	6
2.1.3	The different phases depending on v and t	7
2.2	Doping	7
2.2.1	Ground state	8
2.2.2	Deviations from ground state	9
2.2.3	Quasi particles	10
3	Band structure of the dimer model	11
3.1	Energy bands on a square lattice	11
3.2	The energy dispersion	13
3.3	Analytical preparations	14
3.3.1	Peierls substitution	15
3.3.2	Manipulations of the Hamiltonian	16
3.4	Numerical treatment and plot	18
4	Slave bosons	20
4.1	Slave boson construction	20
4.2	Hubbard Stratonovich transformation	22
4.2.1	Spinon hopping χ	23
4.2.2	Spinon pairing Δ	23
4.2.3	Holon-spinon interaction F	24
4.3	Different phases	25
4.4	Gauge invariances	26
4.5	Saddle point	28
4.5.1	$U(1)$ fractionalized Fermi liquid	29
4.5.2	\mathbb{Z}_2 fractionalized Fermi liquid	30
4.5.3	Notes on π - flux state	32
4.6	Gauge fluctuations	34
5	Conclusion and outlook	37
	Bibliography	39

1 Introduction

In the last decades high T_C superconductors have become of high interest for researchers, since for applications it is easier to use super conductivity at higher temperatures instead of having to cool the system down to temperatures below 77K [1]. Materials that show such super-conducting behavior at high temperatures are most prominently cuprates, but recent research shows that also magic angle twisted bilayer graphene seems to be superconducting at high temperatures relative to the microscopic Fermi energy scale as well [2]. Apart from the high temperature superconductivity cuprates also show other interesting phases like the strange metal and pseudogap phase (see also Fig. 1), which are not fully understood yet.

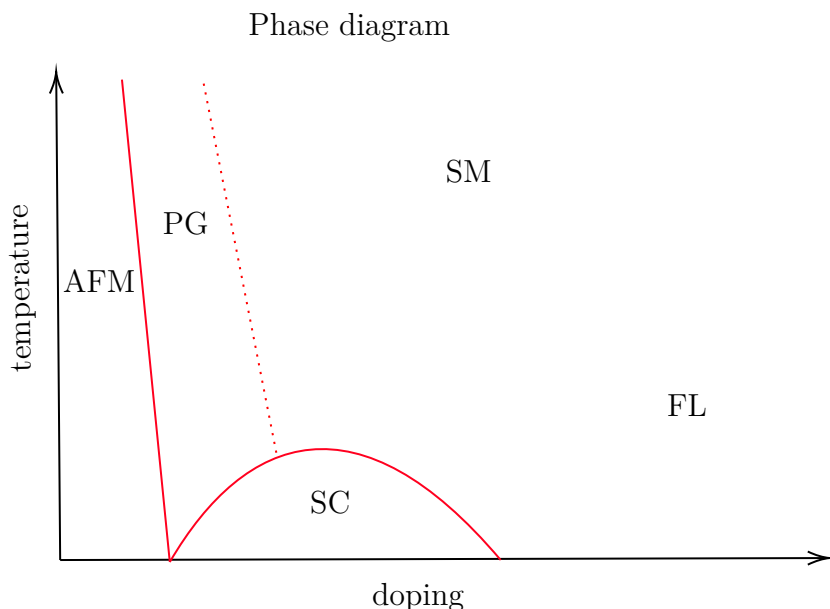


Fig. 1: Schematic phase diagram for cuprates. At half filling and close to half-filling cuprates show anti ferromagnetic (AFM) behavior. Other phases occurring are: the superconducting state (SC), the pseudogap state (PG) and the strange metal (SM). For strong dopings cuprates show Fermi liquid (FL) behavior (based on Ref. [3])

It has been shown that some of the phenomena that happen within the CuO_2 planes of the cuprates can be captured by the t-J model on the square lattice. So one can make use of the basic Hubbard model or its limit the t-J model to investigate the behavior of cuprates (or other high T_C superconductors). Even though those models are very basic in their idea, there is still a lot of ongoing research especially for the states close to the Mott insulator state at half filling. In the strongly interacting

regime there are a lot of different possible ground states depending on, for example, the choice of hopping parameters [4, 5].

To better understand these ground states progress has been made using dynamical mean-field theory [6, 7] and diagrammatic Monte-Carlo methods [8]. Both of those methods were able to show that there is a pseudogap at the edges of the Brillouin zone for a two dimensional square lattice below half filling [9, 10].

There have been approaches to further investigate the properties of the pseudogap state using a dimer model, since the the resonating valence bond (RVB) state [11] seems to be the energetically favorable state for small dopings. In the pseudogap metal excitations carrying both spin and charge cannot be localized on a single lattice site. Therefore, a dimer description is the simplest possibility to describe it [12].

The dimer model is able to capture some of the properties which were experimentally found in pseudogap metals. For example it is able to reproduced the experimentally observed Fermi arcs [13–15]. Furthermore, it is able to reproduce the broken Luttinger relation for pseudogap metals [16].

Another possible approach to get a better understanding of the pseudogap phase is the slave boson approach, which has been shown to be a powerful analytical tool [17, 18]. In the slave boson method the electron operator is represented in terms of a fermionic spinon carrying the electron spin and a slave boson keeps track of the missing charge relative to half-filling, if the system is doped with holes [19]. This separation of spin and charge is not conform with experiments [14, 20]. To circumvent this problem, spinons and holons will be put together to two-particle bound states which carry both spin and charge [21]. There have been introduced two separate ways to achieve these bound states, both being in better agreement with experiments as the treatment without the bound states [22, 23].

The first part of this thesis deals with the magnetic response of magic angle twisted bilayer graphene, which was quite recently found to have superconducting behavior for high temperatures (relative to the microscopic Fermi energy scale) [2]. Its properties have, for example, been investigated in Ref. [24]. We will show that at least some of the effects occurring in twisted bilayer graphene can be explained through the dimer model proposed in Ref. [12] modified for a triangular lattice. While it has already been shown that the dimer model directly induces a small Fermi surface [25], there are other effects like the band splitting when introducing a magnetic field which will be derived in this work. The method used for this will be similar to the one that was used for the famous Hofstadter butterfly plot [26].

In the next part of this thesis the focus will be more on the general understanding of the different phases observed in cuprates. Starting from a slave boson description we will try to obtain a description of the strange metal and pseudogap phase in terms of dimers on a square lattice. Those phases can be described by a so called fractionalized Fermi liquid (FL^{*}) which can be either a U(1)-FL^{*} or a \mathbb{Z}_2 -FL^{*}. This description is able to capture the small Fermi surface of the pseudogap phase.

The remaining thesis is structured as follows: In Chap. 2 the theoretical background, namely the dimer description, will be described in depth, so that in Chap. 3 that

description can be used to obtain the band structure of electrons close to half filling on a triangular lattice. In Chap. 4 a slave boson description will be used to investigate the different phases for the t-J model on a square lattice.

2 Dimers on the square and the triangular lattice

To describe electrons on a lattice one usually uses the fermionic operators $c_{x,\sigma}^\dagger/c_{x,\sigma}$ (with the usual commutation relations) which create/annihilate an electron with spin σ on the site x of the lattice. Their dynamics is often described by a simple Hubbard Hamiltonian (see Ref. [27]) which takes a two particle interaction with strength U at each lattice site into account and allows for hopping between neighboring sites (associated with the parameter J). The Hamiltonian of the Hubbard model reads:

$$H = -J \sum_{\langle i,j \rangle, \sigma} c_{i,\sigma}^\dagger c_{j,\sigma} + U \sum_i c_{i,\uparrow}^\dagger c_{i,\uparrow} c_{i,\downarrow}^\dagger c_{i,\downarrow} \quad (1)$$

where $\langle i, j \rangle$ denotes nearest neighbors. In the second part of this thesis we focus on this model on the square lattice in two spatial dimensions close to half filling, i.e. close to the anti ferromagnetic state. For this one takes the limit of strong correlations $U \gg J$ and U positive to obtain the t-J model (see Ref. [28]). If one takes the number of electrons per site to 1, i.e. half filling, the t-J model reduces to a Heisenberg model, which features an antiferromagnetic ground state on the square lattice. The t-J model will be used for the slave boson description in Sec 4, but in the following sections we will first introduce an alternative description of the problem using dimers.

2.1 Bosonic Dimers

To describe and understand high T_C superconductors the description of electron creation and annihilation operator is not very useful, since the occurring problems can become difficult or even impossible to solve. Therefore we will switch to a dimer description, in which the configuration of two neighboring lattice sites will be described by one dimer. This change in description helps to simplify the calculations. It is based on Anderson's model of resonating valence bond (RVB) state, for which two neighboring electrons form a valence bond (see also Ref. [29]). At half filling this model is not able to describe the antiferromagnetic state, it only features short distance anti ferromagnetic correlations. But: In this theory when doping the half filled system the electrons form Cooper pairs and the RVB state becomes energetically more favorable than the anti ferromagnetic state. Therefore, the dimer description at half filling is introduced by using bosonic dimers in this section, while

in Section 2.2 fermionic dimers will be added to the system to introduce doping from the half filled case.

2.1.1 Introduction and naming

Even though the resonating valence bond state is not able to explain the anti ferromagnetic at half filling, the description with dimers at half filling is a good starting point before adding doping. For this we define the dimers in accordance with Anderson's RVB state using the following considerations:

At half filling there is on average one electron per site. So a dimer will be defined as two neighboring sites occupied by two electrons in total. Two electrons on neighboring sites are spin paired to lower their energy which leads to the dimer being bosonic and free of spin. The dimer creation operator can then be written as (see also Ref. [12]):

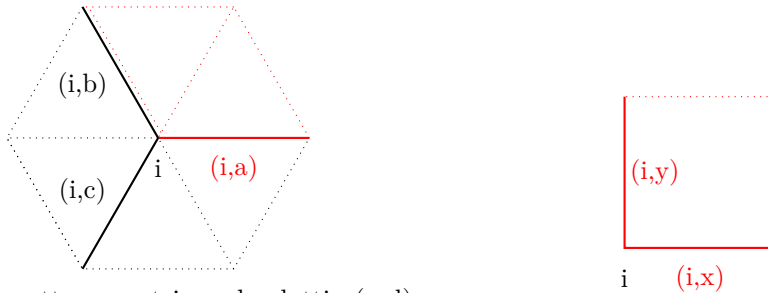
$$D_{i,\eta}^\dagger = \frac{1}{\sqrt{2}}(c_{i,\uparrow}^\dagger c_{i+\eta,\downarrow}^\dagger - c_{i,\downarrow}^\dagger c_{i+\eta,\uparrow}^\dagger) \quad (2)$$

which carries a charge of $2e^-$. Instead of an index (i, j) with i and j nearest neighbors the indices i, η are used corresponding to the points $(i, i + \eta)$, where η is the vector between the two neighboring sites. For simplicity the lattice constant is chosen to be 1. For a square lattice the allowed vectors for η are \vec{e}_x and \vec{e}_y . To prevent double counting the allowed vectors for $\vec{\eta}$ on a triangular lattice are (see Fig. 2):

$$\vec{a} = (1, 0)^T \quad (3)$$

$$\vec{b} = (-1/2, +\sqrt{3}/2)^T \quad (4)$$

$$\vec{c} = (-1/2, -\sqrt{3}/2)^T \quad (5)$$



(a) Plaquette on a triangular lattice (red) and the vectors spanning the lattice: $\vec{a} = (1, 0)^T$, $\vec{b} = (-1/2, +\sqrt{3}/2)^T$ and $\vec{c} = (-1/2, -\sqrt{3}/2)^T$

(b) Plaquette on a square lattice and the vectors spanning the plaquette: $\vec{e}_x = (1, 0)^T$ and $\vec{e}_y = (0, 1)^T$.

Fig. 2: The structure and naming of the vectors spanning the lattice. One plaquette is marked in red, in the triangular lattice two other plaquettes can be obtained by rotating the red plaquette by 120° clockwise or counterclockwise. If the original bond vector is η the vector one obtains through a clockwise rotation of 120° will be denoted by η^+ . For the counterclockwise rotation the notation η^- will be used.

Since only short range interactions will be considered, breaking the system into so called plaquettes which contain four neighboring lattices sites occupied by two dimers is helpful. For the square lattice such a division of the lattice is trivial. For the triangular lattice one has to note that there are three possible plaquettes with different orientations, which are needed to describe the whole lattice in terms of plaquettes (see also Fig. 2).

Checking the commutation relations for the dimers shows that there is the problem that the defined dimer operators are not fully bosonic, since the commutation relation

$$[D_{x,y}, D_{x',y'}^\dagger] = \delta_{xx',yy'} + \delta_{xy',yx'} + \text{restterm} \quad (6)$$

is not the wished for commutation relation (see also Ref. [30]). The exact form of the rest term is not of big importance here, but it is small compared to the first two term, so that it will be neglected and the dimer operator will from now on be considered a bosonic operator.

Since we want to describe the system at half filling we need a way to enforce half filling. To achieve this a hard core constraint will be imposed on the dimers forbidding them to overlap. Otherwise the condition for half-filling would be less obvious to incorporate and the hard core constraint can also easily be pictured.

2.1.2 RK Hamiltonian

The dimers introduced in the previous section will now be used to describe the behavior of the electrons on the lattice. The most general Hamiltonian which can be obtained from the dimers defined above would be one that considers all possible transitions from any one state into any other state.

Even though such a Hamiltonian would be the complete description it is easier to work with the Rokhsar-Kivelson Hamiltonian (also RK-Hamiltonian, see Ref. [31]) which allows only local interaction on a plaquette. It takes into account a repulsion term for each plaquette and a flip of the dimers on the plaquette. For the square lattice it is:

$$H_{RK} = -t \sum_i (|\overline{\square}\rangle \langle \square| + |\square\rangle \langle \overline{\square}|) + v \sum_i (|\overline{\square}\rangle \langle \overline{\square}| + |\square\rangle \langle \square|) \quad (7)$$

The RK-Hamiltonian on the triangular lattice is:

$$H_{RK} = -t \sum_{i,\eta} (|\overline{\triangle}\rangle \langle \triangle| + |\triangle\rangle \langle \overline{\triangle}|) + v \sum_{i,\eta} (|\overline{\triangle}\rangle \langle \overline{\triangle}| + |\triangle\rangle \langle \triangle|) \quad (8)$$

The state the system is in strongly depends on the choice of the parameters v and t . Therefore, we will look at the possible choices for these parameters in the following subsection to get an overview of the most important possible states.

2.1.3 The different phases depending on v and t

Depending on the choice of the parameters v and t in Eq. 8 and Eq. 7 we have different phases (see Fig. 3). The most prominent phases occurring both on the square and the triangular lattice are (see also Ref. [32]):

- staggered phase: For $v > |t|$ one has the so called staggered phase which has a ground state without any flippable plaquettes.
- columnar phase: For $v < -|t|$ one has the so called columnar phase which has as a ground state the state with the most flippable plaquettes possible.
- RVB state: For $v = \pm t$, which is also called Rokhsar-Kivelson (RK) point (or RK line), one has the resonating valence bond (RVB) state as ground state which is degenerate. On the square lattice the RVB state occurs only at the RK point, but on the triangular lattice the RVB state extends to other regions close to the RK-point as long as the gauge symmetry of the system is not broken.

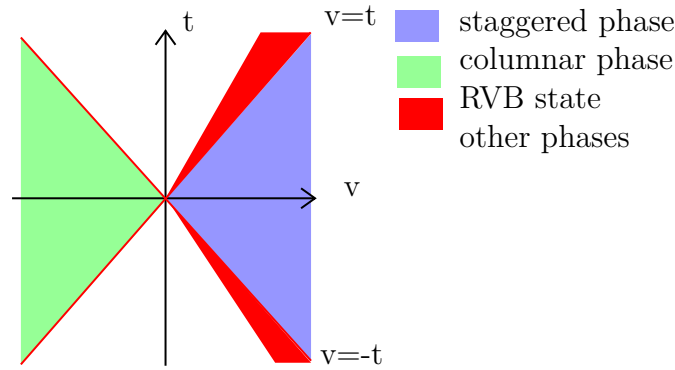


Fig. 3: Phase diagram for the RK model on a triangular lattice for the different choices of v and t . For the square lattice the RVB state only occurs exactly at the RK line $v = \pm t$. Apart from the staggered and columnar phase and the RVB state the other phases strongly depend on the lattice symmetry. For a square lattice one has the plaquette state, while for a triangular lattice one has the so called $\sqrt{12} \times \sqrt{12}$ state and possibly other states as well [32].

In the following section we will look at the RK point, since it is the best understood case, and will add some doping to the system. Later on also a perturbation from the RK point will be added (see Sec 2.2.2).

2.2 Doping

To the description at half filling some doping will be added now, since this will allow us to reach a description of the superconducting phase and other interesting phases. To achieve a description away from half filling the system will be doped by

exchanging the bosonic dimers for fermionic dimers which are a superposition of a hole and an electron. The fermionic dimer operator can be written as (see also Ref. [12]):

$$F_{(i,\eta),\sigma}^\dagger = \frac{1}{\sqrt{2}}(c_{i,\sigma}^\dagger + c_{i+\eta,\sigma}^\dagger) \quad (9)$$

and fulfils the usual anti commutator relations.

Now the system of bosonic dimers at the RK point will be doped with few fermionic dimers. At the RK point $v = t$ the RK-Hamiltonian in Eq. 8 can be simplified and can be written as a sum of projectors. For the doping an interaction term between the bosonic and fermionic operators will be added to the system. Similar to the undoped RK Hamiltonian all possible flips and swaps on a plaquette with one fermionic and one bosonic dimer ($\overline{\blacksquare}$, $\overline{\square}$, \blacktriangledown and \blacktriangleleft with red = fermionic dimer and black = bosonic dimer) will be taken into account. Since it is difficult to work with all those terms we will start from the exactly solvable Hamiltonian, which is just a sum of projectors, and then add a perturbation, such that it is physical. Since the treatment in Chap. 3 is only on the triangular lattice the corresponding Hamiltonian is given here:

$$H = H_{RK} + H_{int} \quad (10)$$

$$H_{RK} = v \sum (|\overline{\blacksquare}\overline{\square}\rangle - |\blacktriangledown\blacktriangleleft\rangle)(\langle\overline{\blacksquare}\overline{\square}| - \langle\blacktriangledown\blacktriangleleft|) \quad (11)$$

$$H_{int} = v \sum (|\overline{\blacksquare}\overline{\square}\rangle + |\overline{\square}\overline{\blacksquare}\rangle - |\blacktriangledown\blacktriangleleft\rangle - |\blacktriangleleft\blacktriangledown\rangle)(\langle\overline{\blacksquare}\overline{\square}| + \langle\overline{\square}\overline{\blacksquare}| - \langle\blacktriangledown\blacktriangleleft| - \langle\blacktriangleleft\blacktriangledown|) \quad (12)$$

We only look at small dopings therefore we do not consider a term with fermion-fermion interactions on a plaquette, since the probability of two fermionic dimers being on the same plaquette is negligible.

In this Hamiltonian the prefactors of all the terms have the same value, which is easy to work with but is not completely physical, since this case does not coincide with the Hubbard model as dimer swaps and plaquette flips do not happen with the same amplitude. Therefore, a perturbation will be added later on in Sec. 2.2.2 to adjust the dimer model to be the same as the Hubbard model. But for now it is useful to look at the problem for Eq. 10 because then the Hamiltonian is a sum of projectors which implies that all eigenvalues have to be null or larger, which means that the ground state energy is 0.

2.2.1 Ground state

We are interested in the ground state of the Hamiltonian in Eq. 10, which has an energy of 0 due to the Hamiltonian being a sum of projectors. The the ground state for two fermionic dimers in a background of bosonic dimers itself has been determined by Brin Verheijden in his thesis (see Ref [30]) as:

$$|p_1, p_2\rangle = \sum_{i_1, \eta_1, i_2, \eta_2} C_{\eta_1}(p_1) C_{\eta_2}(p_2) e^{i(p_1 \cdot i_1 + p_2 \cdot i_2)} |(i_1, \eta_1), (i_2, \eta_2)\rangle \quad (13)$$

with:

$$C_\eta(p) = \frac{q}{\sqrt{N}} \frac{1 + e^{ip \cdot \eta}}{\sum_\eta |1 + e^{ip \cdot \eta}|^2} \quad (14)$$

Note that $q = 6$ and N is the number of lattice points. This is the ground state for 2 fermionic dimers in the system, but it can easily be extended to N fermionic dimers (N holes). In that case one has:

$$|p_1, \dots, p_N\rangle = \sum_{i_1, \eta_1, \dots, i_N, \eta_N} \prod_{j=1}^N \left(C_{\eta_j}(p_j) e^{i\eta_j \cdot i_j} \right) |(i_1, \eta_1), \dots, (i_N, \eta_N)\rangle \quad (15)$$

In the following section a small perturbation will now be added to this ground state to better take into account the different transition amplitudes of a plaquette flip and a dimer swap.

2.2.2 Deviations from ground state

Up to now we only looked at the system at the RK-point, since then the Hamiltonian has the convenient feature of being a sum of projectors. Therefore, it is easy to work with, but the assumption that all the terms in the interaction have the same prefactor is not valid, since the flipping of the plaquette and the dimer swap do not happen with the same amplitude, as will be shown now:

When allowing only nearest neighbor hopping the amplitudes for a dimer swap and and plaquette flip are not the same on a triangular lattice. The amplitude for a dimer swap is $-3/4t$, while the plaquette flip happens with an amplitude of $1/2t$, where t is the hopping amplitude for a single electron.

Therefore one has to add a perturbation to the ground state. For this the following perturbation is added to the Hamiltonian:

$$\Delta H = -\delta_u \sum_{j, \eta} \sum_{\square = \{+, -\}} F_{j+\eta^\square, \eta}^\dagger D_{j, \eta}^\dagger D_{j+\eta^\square, \eta} F_{j, \eta} \quad (16)$$

with $\delta_u = -1/2v$ so that it takes into account the larger amplitude for the dimer swap. Here η^+ and η^- indicate the orientation of the lattice vector compared to the orientation of η , i.e. $\eta^+(\eta^-)$ is η rotated by 120° clockwise (counter clockwise). Adding this perturbation to the Hamiltonian induces a new ground state energy (see also Ref [25]):

$$\Delta E = \sum_p \epsilon(p) \quad (17)$$

with

$$\epsilon(p) = -\frac{\delta_u}{6} \sum_\eta \frac{2 \cos(\eta^+ \cdot p) + 2 \cos(\eta^- \cdot p)}{\sum_{\eta'} |1 + e^{i\eta' \cdot p}|^2} \quad (18)$$

Note that the ground state energy is a sum of energies each associated with one momentum. Therefore, in the next section a quasiparticle description will be introduced in which each quasi particle is associated with a momentum p .

2.2.3 Quasi particles

After now having obtained a ground state energy for the problem, we would like to switch to a quasi particle description by defining quasi particles which are associated with a momentum p (see also Ref. [30]). This treatment seems useful, since the ground state energy is a sum of separate energies each corresponding to a momentum p . One can define:

$$|p_1, p_2, \dots, p_n\rangle = \prod_i f_{p_i}^\dagger |0^*\rangle \quad (19)$$

$$f_p^\dagger = C_\eta(p) e^{i\vec{p}\cdot\vec{\eta}} F_{i\eta}^\dagger D_{i\eta} \quad (20)$$

$$H_p |p_1 \dots p_n\rangle = \sum_{i=1}^n \epsilon(p_i) |p_1 \dots p_n\rangle \quad (21)$$

where $|0^*\rangle$ is the ground state of the RK Hamiltonian without any fermionic dimers in the system and $C_\eta(p)$ as in Eq. 14. It would be nice to be able to write:

$$H_p = \sum_p \epsilon(p) f_p^\dagger f_p \quad (22)$$

but for this to make sense the quasi particle operator has to be perfectly fermionic. This is not for all momenta the case, therefore this description is only valid for the momentum space where the quasiparticle operator is perfectly fermionic. In this space one can also relate the quasi particle operator to electron annihilation operator with:

$$f_p^\dagger = K(p) c_{-p} \quad (23)$$

with

$$K(p) = \frac{6}{\sum_\eta |1 + e^{i\vec{p}\cdot\vec{\eta}}|} \quad (24)$$

This is a very useful result to link our quasiparticles to the electronic operators.

3 Band structure of the dimer model

After having introduced the idea of the dimer model on a triangular lattice, we now can start working with it. The reason we focussed on the triangular lattice is that in magic angle twisted bilayer graphene, which is super conducting at relatively high temperatures, the two graphene sheets form a triangular super lattice (see Fig. 4).

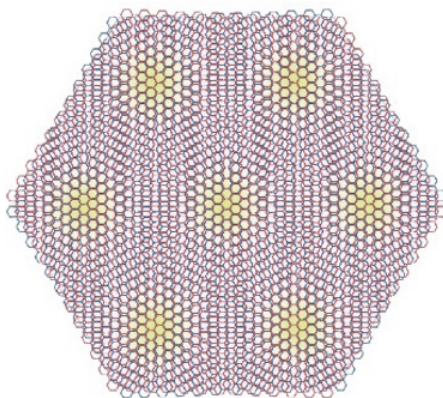


Fig. 4: Two sheets of graphene placed on each other and twisted in by the magic angle of about 1.1° form a triangular superlattice. This triangular super lattice will be used to explain the magnetic response of the twisted bilayer graphene. (Source of the figure: Ref. [33])

Since this triangular super lattice is the main feature of twisted bilayer graphene, we will use it as a starting point for better understanding the physics happening in the material. For this the dimer description introduced in Chap. 2 will be used. The energy spectrum of a triangular lattice has already been determined by Brin Verheijden in his thesis (see also Ref. [25]) and we will now deepen our understanding of the problem. For this we will focus here on the magnetic response of the system and are especially interested in the energy spectrum when introducing a magnetic field. Since the same method as Hofstadter used to obtain his famous butterfly plot be used to achieve this, it will be briefly described in the next section before it is then applied on a triangular lattice using the dimer description.

3.1 Energy bands on a square lattice

Before starting with the calculations it makes sense to briefly remind the reader of the Hofstadter butterfly and how it was originally obtained in Ref. [26].

Hofstadter wanted to investigate Bloch electrons on a square lattice in a magnetic field and found a trick for solving the problem by solving it for specific rational magnetic fields and then deducing the complete energy spectrum from it.

To achieve this he started from Bloch electrons with energy function:

$$W(\vec{k}) = 2E_0(\cos k_x a + \cos k_y a) \quad (25)$$

and replace k by using a Peierls substitution:

$$\hbar\vec{k} \rightarrow \vec{p} - \frac{e}{c}\vec{A} \quad (26)$$

where \vec{A} is the magnetic field which has been chosen in the Landau gauge with $\vec{A} = Bx\vec{e}_y$. He used this in the time independent Schrödinger equation which he simplified by assuming plane wave behavior of the eigenfunction φ in one spatial dimension. He then obtained a problem of the form:

$$\vec{V}_{n+1} = M_n \vec{V}_n \quad (27)$$

where \vec{V} is $(\varphi_n, \varphi_{n-1})^T$ and

$$M_n = \begin{pmatrix} E - 2 \cos(2\pi n\phi - l) & -1 \\ 1 & 0 \end{pmatrix} \quad (28)$$

where E is the eigenenergy of the Hamiltonian, ϕ and l are constants. Note that ϕ depends on the strength of the magnetic field. Hofstadter then used the fact the M was periodic to draw some conclusions for the eigenvalues of $Q = \prod_i M_{n+i}$ for ϕ being a fraction. He obtained that the sum of the absolute values of the eigenvalues of Q has to fulfill:

$$\text{Tr}(|Q|) \leq 2 \quad (29)$$

Using this condition allowed him to plot the physical energies for fractional choices of ϕ , which resulted in the energy spectrum called the Hofstadter's butterfly (see Fig. 5).

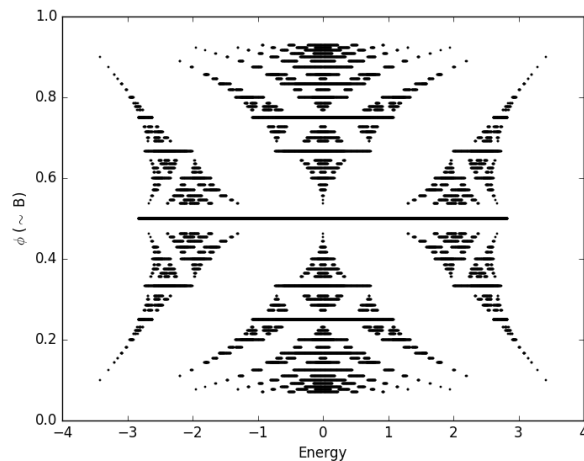


Fig. 5: Hofstadter's butterfly. Plot of the energy bands for fractional values of ϕ . Through analytic continuation the band structure can be extended to all values of ϕ .

The plot Hofstadter obtained showed the energy bands for different choices of the magnetic field (since ϕ contains the magnetic field strength). Due to the shape, the plot is called Hofstadter's butterfly.

In the following we will use the similar proceeding for our problem on the triangular lattice.

3.2 The energy dispersion

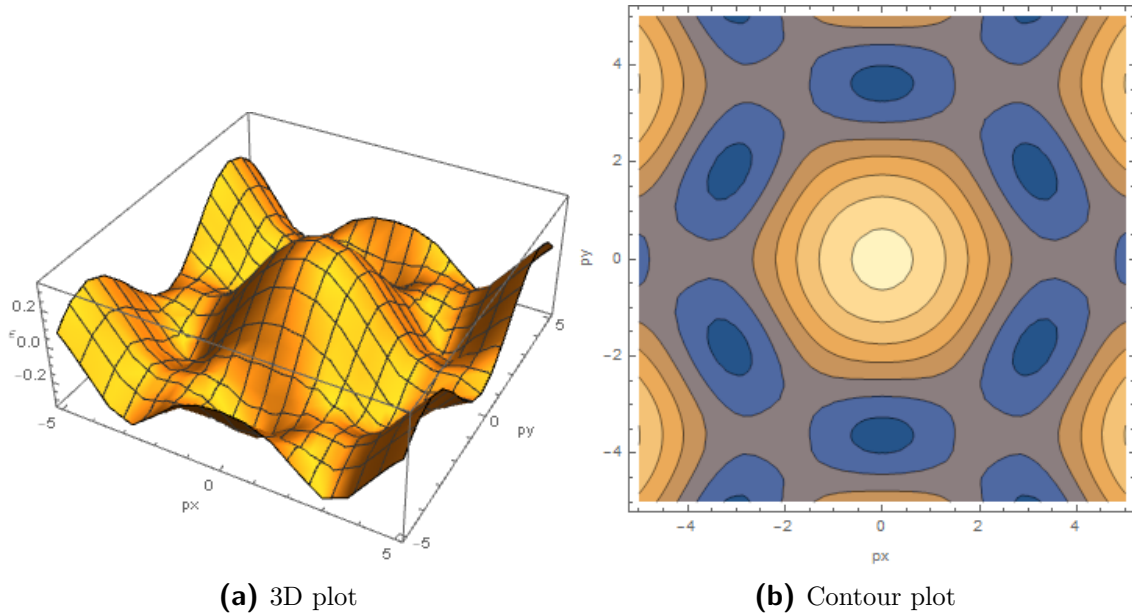


Fig. 6: Energy dispersion for the quasiparticles (Eq. 18)

After now having obtained a basic understanding of the Hofstadter's butterfly method, we can start to apply and adapt it to our own problem. The starting point is the quasiparticle Hamiltonian in Eq. 22 and the dispersion relation in Eq. 18 and see how the quasiparticles behave on introducing a magnetic field. The energy dispersion is displayed in Fig. 6 using a 3D plot and a contour plot.

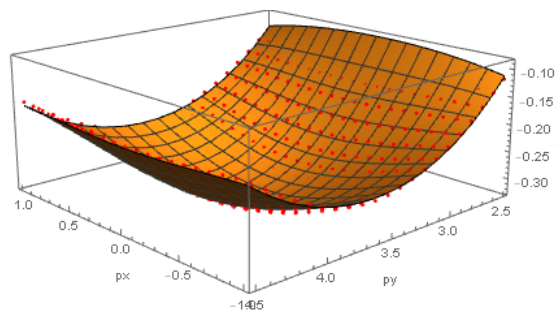


Fig. 7: The energy dispersion from Eq. 18 (orange) has been fitted to an equation of the form of Eq. 30 (red dots) around the minimum at $\vec{p} = (0, \frac{2\pi}{\sqrt{3}})^T$

The energy dispersion in Eq. 18 is of a quite complicated form, which makes analytic treatment difficult. Therefore, we will try to approximate it by a tight-binding dispersion with nearest, and next-nearest neighbor terms with a function of the form:

$$\epsilon(p) \approx \delta_u \left(t_0 + t_1 \sum_{\eta} \cos(\eta \cdot p) + \frac{t_2}{2} \sum_{\eta \neq \eta'} \cos(\eta \cdot p) \cos(\eta' \cdot p) \right) \quad (30)$$

The energy dispersion omits several minima, but it is symmetric so we will just choose the minimum at $\vec{p} = (0, \frac{2\pi}{\sqrt{3}})^T$. Around the other minima at $(\pi, \frac{\pi}{\sqrt{3}})^T$, $(-\pi, \frac{\pi}{\sqrt{3}})^T$, $(\pi, -\frac{\pi}{\sqrt{3}})^T$, $(-\pi, -\frac{\pi}{\sqrt{3}})^T$ and $(0, \frac{2\pi}{\sqrt{3}})^T$ the energy dispersion has the same form (up to a rotation around the origin). Fitting Eq. 30 to the energy dispersion at the chosen minimum yields the following fitting parameters:

$$t_0 = -0.124586 \quad (31)$$

$$t_1 = -0.479846 \quad (32)$$

$$t_2 = -0.296818 \quad (33)$$

The fit is displayed in Fig. 7 and one sees that the actual energy dispersion (orange) is well in accordance with the fit (red dots).

After this simplification it is now possible to go on with the same proceeding as for the original Hofstadter's butterfly. In the following sections the simplified energy dispersion will now be used for the analytical treatment. A magnetic field will now be added to the system to understand the magnetic response, before the problem will be plotted in the end of this chapter.

3.3 Analytical preparations

To be able to plot the energy bands for the triangular lattice in a Hofstadter butterfly like plot the Hamiltonian, eigenfunctions and eigenvalues have to be manipulated accordingly. For this the Hamiltonian from Eq. 22 will be combined with the approximated energy dispersion in Eq. 30.

Using this the Hamiltonian will now be Fourier transformed. This yields the following Hamiltonian in position space:

$$H = \delta_u \sum_l [t_0 f_l^\dagger f_l + \frac{t_1}{2} \sum_{\eta} (f_l^\dagger f_{l+\eta} + f_l^\dagger f_{l-\eta}) + \frac{t_2}{8} \sum_{\eta \neq \eta'} (f_l^\dagger f_{l-\eta-\eta'} + f_l^\dagger f_{l-\eta+\eta'} + f_l^\dagger f_{l+\eta-\eta'} + f_l^\dagger f_{l+\eta+\eta'})] \quad (34)$$

In the following we will now add a magnetic field to this Hamiltonian using a Peierls substitution and then take a look at the eigenvalue problem arising from the Schrödinger equation. This can then be used in Sec. 3.4 to make a Hofstadter butterfly like plot.

3.3.1 Peierls substitution

After obtaining the Hamiltonian in position space, a magnetic field perpendicular to the lattice plane is now added to the system, so that the magnetic response can be surveilled. To keep the calculations simple the following gauge for the vector potential \vec{A} is chosen:

$$\vec{A} = By\vec{e}_x. \quad (35)$$

It fulfils the Landau gauge, which breaks translational symmetry in y- direction, but does not change the underlying physics. Using a Peierls substitution [34] this magnetic field changes each of the terms in the Hamiltonian by a factor

$$\exp\left(-\frac{e}{\hbar} \int_j^l \vec{A} \cdot d\vec{r}\right) \quad (36)$$

where j and l denote the different positions and $d\vec{r}$ denotes a line segment. Evaluating the integral in the line integral gives:

$$\int_j^l \vec{A} \cdot d\vec{r} = B [(\vec{l} - \vec{j}) \cdot \vec{e}_x] \left[\left(\frac{\vec{l} + \vec{j}}{2} \right) \cdot \vec{e}_y \right] \quad (37)$$

It is important to note, that \vec{l} and \vec{j} are the cartesian coordinates of the lattice points. It makes sense to parametrize the lattice points in terms of two of the vectors spanning the lattice (here \vec{a} and $-\vec{c}$ have been chosen). Then one can write the lattice point \vec{l} as:

$$\vec{l} = n_x \vec{a} - n_y \vec{c} = (n_x + \frac{1}{2}n_y)\vec{e}_x + \frac{\sqrt{3}}{2}n_y \vec{e}_y \quad (38)$$

To avoid long equations later on it makes sense to already take a look at all the terms which occur for a given \vec{l} . For $\vec{j} = \vec{l}$ one does not have to a factor, but one obtains one in the cases:

$$\begin{aligned} \vec{j} = \vec{l} \pm \vec{a} & \quad \theta_{lj} = \pm \frac{2\pi Be}{h} n_y \frac{\sqrt{3}}{2} & \quad n_x \pm 1, n_y \\ \vec{j} = \vec{l} \pm \vec{b} & \quad \theta_{lj} = \mp \frac{2\pi Be}{h} \frac{1}{2} \frac{\sqrt{3}}{2} (n_y \pm \frac{1}{2}) & \quad n_x \mp 1, n_y \pm 1 \\ \vec{j} = \vec{l} \pm \vec{c} & \quad \theta_{lj} = \mp \frac{2\pi Be}{h} \frac{1}{2} \frac{\sqrt{3}}{2} (n_y \mp \frac{1}{2}) & \quad n_x, n_y \mp 1 \\ \vec{j} = \vec{l} \pm \vec{a} \pm \vec{b} & \quad \theta_{lj} = -\frac{2\pi Be}{h} (\mp 1 \pm \frac{1}{2}) \frac{\sqrt{3}}{2} (n_y \pm \frac{1}{2}) & \quad n_x \pm 1 \mp 1, n_y \pm 1 \\ \vec{j} = \vec{l} \pm \vec{a} \pm \vec{c} & \quad \theta_{lj} = -\frac{2\pi Be}{h} (\mp 1 \pm \frac{1}{2}) \frac{\sqrt{3}}{2} (n_y \mp \frac{1}{2}) & \quad n_x \pm 1, n_y \mp 1 \\ \vec{j} = \vec{l} \pm \vec{b} \pm \vec{c} & \quad \theta_{lj} = -\frac{2\pi Be}{h} (\pm \frac{1}{2} \pm \frac{1}{2}) \frac{\sqrt{3}}{2} (n_y \mp \frac{1}{2} \mp \frac{1}{2}) & \quad n_x \mp 1, n_y \pm 1 \mp 1 \end{aligned} \quad (39)$$

where the last column gives the the coordinates of \vec{j} with respect to the reparametrized vector \vec{l} .

After having determined all the relevant factors we can now add this to the Hamiltonian and go on to look on the eigenvalue equation.

3.3.2 Manipulations of the Hamiltonian

After now having determined the prefactors which have to be added for the Peierls substitution it is time to look at the eigenvalue problem. Applying the modified Hamiltonian to an eigenfunction now yields:

$$\begin{aligned}
E\psi_{m_x, m_y} = \delta_u \left\{ & t_0 \psi_{m_x, m_y} \right. \\
& + \left(\frac{t_1}{2} e^{i \frac{2\pi B}{\phi_0} m_y \frac{\sqrt{3}}{2}} + \frac{t_2}{4} e^{i \frac{2\pi B}{\phi_0} 2\frac{1}{2} \frac{\sqrt{3}}{2} m_y} \right) \psi_{m_x+1, m_y} \\
& + \left(\frac{t_1}{2} e^{-i \frac{2\pi B}{\phi_0} m_y \frac{\sqrt{3}}{2}} + \frac{t_2}{4} e^{-i \frac{2\pi B}{\phi_0} 2\frac{1}{2} \frac{\sqrt{3}}{2} m_y} \right) \psi_{m_x-1, m_y} \\
& + \left(\frac{t_1}{2} e^{-i \frac{2\pi B}{\phi_0} \frac{1}{2} (m_y + \frac{1}{2}) \frac{\sqrt{3}}{2}} + \frac{t_2}{4} e^{-i \frac{2\pi B}{\phi_0} (1 - \frac{1}{2}) (m_y + \frac{1}{2}) \frac{\sqrt{3}}{2}} \right) \psi_{m_x-1, m_y+1} \\
& + \left(\frac{t_1}{2} e^{i \frac{2\pi B}{\phi_0} \frac{1}{2} (m_y - \frac{1}{2}) \frac{\sqrt{3}}{2}} + \frac{t_2}{4} e^{i \frac{2\pi B}{\phi_0} (1 - \frac{1}{2}) (m_y - \frac{1}{2}) \frac{\sqrt{3}}{2}} \right) \psi_{m_x+1, m_y-1} \\
& + \left(\frac{t_1}{2} e^{-i \frac{2\pi B}{\phi_0} \frac{1}{2} (m_y - \frac{1}{2}) \frac{\sqrt{3}}{2}} + \frac{t_2}{4} e^{-i \frac{2\pi B}{\phi_0} (1 - \frac{1}{2}) (m_y - \frac{1}{2}) \frac{\sqrt{3}}{2}} \right) \psi_{m_x, m_y-1} \\
& + \left(\frac{t_1}{2} e^{i \frac{2\pi B}{\phi_0} \frac{1}{2} (m_y + \frac{1}{2}) \frac{\sqrt{3}}{2}} + \frac{t_2}{4} e^{i \frac{2\pi B}{\phi_0} (1 - \frac{1}{2}) (m_y + \frac{1}{2}) \frac{\sqrt{3}}{2}} \right) \psi_{m_x, m_y+1} \\
& + \left(\frac{t_2}{4} e^{i \frac{2\pi B}{\phi_0} (1 + \frac{1}{2}) \frac{\sqrt{3}}{2} (m_y + \frac{1}{2})} \right) \psi_{m_x+1, m_y+1} \\
& + \left(\frac{t_2}{4} e^{-i \frac{2\pi B}{\phi_0} (1 + \frac{1}{2}) \frac{\sqrt{3}}{2} (m_y - \frac{1}{2})} \right) \psi_{m_x-1, m_y-1} \\
& + \left(\frac{t_2}{4} e^{i \frac{2\pi B}{\phi_0} (1 + \frac{1}{2}) \frac{\sqrt{3}}{2} (m_y - \frac{1}{2})} \right) \psi_{m_x+2, m_y-1} \\
& + \left(\frac{t_2}{4} e^{-i \frac{2\pi B}{\phi_0} (1 + \frac{1}{2}) \frac{\sqrt{3}}{2} (m_y + \frac{1}{2})} \right) \psi_{m_x-2, m_y+1} \\
& + \frac{t_2}{4} \psi_{m_x+1, m_y-2} \\
& \left. + \frac{t_2}{4} \psi_{m_x-1, m_y+2} \right\} \tag{40}
\end{aligned}$$

where $\frac{B\sqrt{3}}{4\phi_0}$ will be replaced by ϕ . Since the exponential prefactors only depend on the y-position we can write the eigenfunction as

$$\psi = e^{ik_x m_x} \varphi(m_y) \tag{41}$$

In the original paper by Hofstadter [26] from this now a matrix was constructed and through a condition on its trace the physical energies have been found. This is not

feasible in this case due to the fact that the trace as well as its bound are dependent on k_x . To avoid this problem we will use the approach introduced by Langbein in Ref. [35], which also has been used to find the band structures of several other lattices (e.g. see Ref. [36] or Ref. [37]).

The approach proposed by Langbein also uses the fact that for rational choices of $\phi = p/q$ the eigenvalue equation is the same for the m th and the $(m+q)$ th lattice point, so that one has:

$$\varphi_m = e^{i2\pi l} \varphi_{m+q} \quad (42)$$

This means that for each q we have q different eigenvalue equations, which will be written in matrix form:

$$M \begin{pmatrix} \varphi_m \\ \vdots \\ \varphi_{m+q-1} \end{pmatrix} = 0 \quad (43)$$

with

$$M = \begin{pmatrix} C_m & D_m & E_m & \dots & A_m e^{-i2\pi l} & B_m e^{-i2\pi l} \\ B_{m+1} & C_{m+1} & D_{m+1} & E_{m+1} & \dots & A_{m+1} e^{-i2\pi l} \\ \vdots & & & & & \vdots \\ D_{m+q-1} e^{i2\pi l} & E_{m+q-1} e^{i2\pi l} & \dots & A_{m+q-1} & B_{m+q-1} & C_{m+q-1} \end{pmatrix} \quad (44)$$

where

$$\begin{aligned} A_m &= \frac{t_2}{4} e^{ik_x} \\ B_m &= \frac{t_1}{2} e^{i2\pi \frac{p}{q}(m-\frac{1}{2})+ik_x} + \frac{t_1}{2} e^{-i2\pi \frac{p}{q}(m-\frac{1}{2})} \\ &\quad + \frac{t_2}{4} e^{-i2\pi \frac{p}{q}(m-\frac{1}{2})} + \frac{t_2}{4} e^{i2\pi \frac{p}{q}3(m-\frac{1}{2})+i2k_x} \\ &\quad + \frac{t_2}{4} e^{i2\pi \frac{p}{q}(m-\frac{1}{2})+ik_x} + \frac{t_2}{4} e^{-i2\pi \frac{p}{q}3(m-\frac{1}{2})-ik_x} \\ C_m &= -\frac{E}{\delta_u} + t_0 + t_1 \cos\left(2\pi 2\frac{p}{q}m + k_x\right) + \frac{t_2}{2} \cos\left(2\pi 2\frac{p}{q}m + k_x\right) \\ D_m &= \frac{t_1}{2} e^{-i2\pi \frac{p}{q}(m+\frac{1}{2})-ik_x} + \frac{t_1}{2} e^{i2\pi \frac{p}{q}(m+\frac{1}{2})} \\ &\quad + \frac{t_2}{4} e^{i2\pi \frac{p}{q}(m+\frac{1}{2})} + \frac{t_2}{4} e^{-i2\pi \frac{p}{q}3(m+\frac{1}{2})-ik_x} \\ &\quad + \frac{t_2}{4} e^{-i2\pi \frac{p}{q}(m+\frac{1}{2})-ik_x} + \frac{t_2}{4} e^{i2\pi \frac{p}{q}3(m+\frac{1}{2})+ik_x} \\ E_m &= \frac{t_2}{4} e^{-ik_x} \end{aligned} \quad (45)$$

and horizontal dots indicate zeros. In the following section this matrix will be used to obtain a plot of the energy bands.

3.4 Numerical treatment and plot

One is interested in the case where the determinant of M is 0. So in fact one would test if for each choice of energy and p/q , there is a possible choice for k_x and l such that the determinant is zero. This is quite challenging numerically, so instead for each choice of p/q the values of k_x and l for which the determinant is minimal and maximal will be determined and it will be checked for each energy if using the minimal values for k_x and l the determinant is smaller than 0 (or larger than 0 for the maximal values respectively). The energies and ϕ s for which this condition is fulfilled are part of the energy bands. This now gives a proceeding to find the energy bands for different magnetic field strengths $\phi = p/q$.

Using this proceeding we are now able to plot the energy bands for different magnetic fields at the energy minimum, which is displayed in Fig. 8.

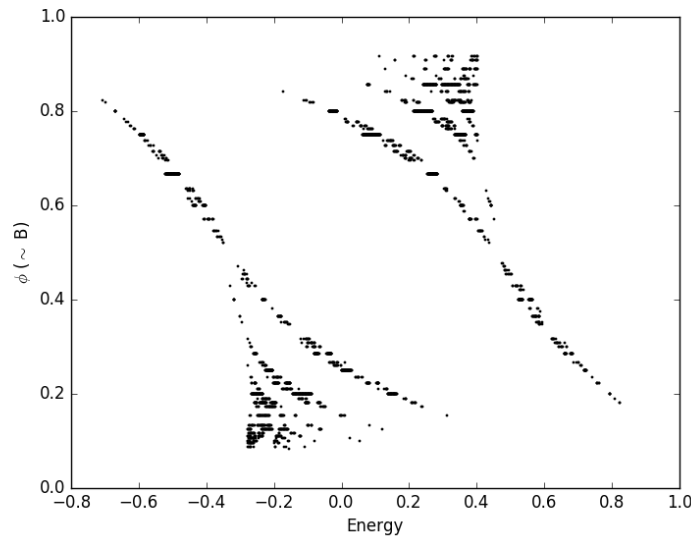


Fig. 8: Energy bands for different magnetic field strengths ($\phi = \frac{B\sqrt{3}}{4\phi_0}$) for momenta close to the minimum of the energy dispersion at $\vec{p} = (0, \frac{2\pi}{\sqrt{3}})^T$

Before taking a closer look, if this plot gives interesting physical results, it makes sense so shortly check if this result is actually plausible or not. This can firstly be done by checking if the number of bands at $1/n$ is n . While for $n = 3$ and $n = 4$ this is clearly valid, there seem to be no bands for $\phi = 1/2$, but this is probably only due to the lack of accuracy of the plot. If there are just two energy points (not ranges) for $\phi = 1/2$ it is unlikely to find them due to numerical rounding.

Another way to check if the plot is plausible to take a look at similar problems and see if the energy bands are indeed similar. For a triangular lattice at $\vec{p} = 0$ the band structure has been plotted several times, e.g. in Ref. [36] or Ref. [38], and is displayed in Fig. 9. To obtain the band structure the following parameters were

chosen:

$$\begin{aligned} t_0 &= 0.129683 \\ t_1 &= -0.30947 \\ t_2 &= 0 \end{aligned} \tag{46}$$

since those parameters are able to fit the dispersion relation (Eq. 18) around $\vec{p} = 0$ using the same proceeding as in Sec. 3.2. One sees that this plot is similar to the band structure at the minimum but not quite the same. Therefore, it can be concluded, that the obtained band structure in Fig. 8 indeed makes sense. Due to the large unit cells in magic angle twisted bilayer graphene, it might now be possible to check these results in experiments.

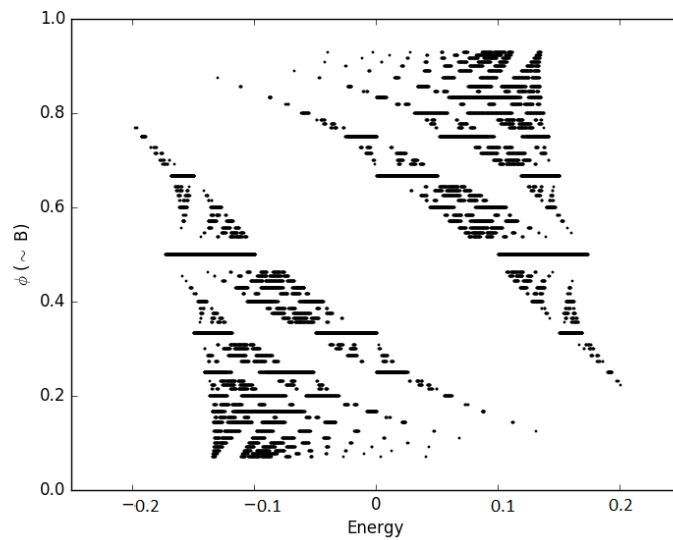


Fig. 9: Hofstadter butterfly plot for a triangular lattice at $\vec{p} = (0, 0)^T$ allowing only nearest neighbor interactions

4 Slave bosons

To get a better understanding of high T_C superconductors we will use a slave boson description, which will simplify the calculations and will therefore give a better understanding of the different phases within a high T_C superconductor (see Ref. [19] Sec.VIII). Since more work has been done on the square lattice we will look at the slave boson description on the square lattice, so that we can easily compare our results to already existing results. For this we will start from the t-J Hamiltonian which reads

$$H = \sum_{\langle i,j \rangle} J \left(\vec{S}_i \cdot \vec{S}_j - \frac{1}{4} n_i n_j \right) - \sum_{i,j,\sigma} t_{ij} (c_{i\sigma}^\dagger c_{j\sigma} + h.c.) \quad (47)$$

where $c_{i\sigma}$ and $c_{i\sigma}^\dagger$ are so called Gutzwiller projected operators in which double occupancy is forbidden. This is used to induce strong Coulomb interactions. The t-J Hamiltonian was derived from the Hubbard model by Jozef Spalek in 1977 (see Ref. [28]) and is still the best description for the anti-ferromagnetic state at half-filling (or close to half-filling). Firstly we will rewrite this Hamiltonian using the slave boson construction and then we will use Hubbard Stratonovich decoupling to deduce the physical behavior of the system. After the Hubbard Stratonovich decoupling the system omits several different phases depending on the decoupling parameters. These phases will be looked upon in detail in the following sections. The focus will be on the not yet well understood states like the pseudogap metal and the strange metal, which can both be described by a fractionalized Fermi liquid as we will see in Sec. 4.5.

4.1 Slave boson construction

The idea of a slave boson description is to rewrite the electron operators $c_{i\sigma}^\dagger$ and $c_{i\sigma}$ in a way that easily allows for the constraint of forbidden double occupation to be taken into account (see Ref. [39]). One rewrites the electron operator as:

$$c_{i\sigma}^\dagger = f_{i\sigma}^\dagger b_i + \epsilon_{\sigma\sigma'} f_{i\sigma'} d_i^\dagger \quad (48)$$

where $\epsilon_{\uparrow\downarrow} = -\epsilon_{\downarrow\uparrow} = 1$ is the antisymmetric tensor. In this representation $f_{i\sigma}^\dagger/f_{i\sigma}$ are fermion operators which carry a spin (therefore now called spinons). b_i and d_i^\dagger are the so called slave bosons. While b_i describes the destruction of a hole on site i (also holon), d_i^\dagger represents the creation of an electron pair. Adding the constraint

$$\sum_{\sigma} f_{i\sigma}^\dagger f_{i\sigma} + b_i^\dagger b_i + d_i^\dagger d_i = 1 \quad (49)$$

for each lattice site i reproduces the correct algebra of the electron operators and ensures that at each site there is zero, one or two electrons. In this representation it is easily possible to forbid double occupancy: one just deletes d_i/d_i^\dagger from the last two equations which then leads to:

$$c_{i\sigma}^\dagger = f_{i\sigma}^\dagger b_i \quad (50)$$

and the constraint then becomes:

$$\sum_{\sigma} f_{i\sigma}^\dagger f_{i\sigma} + b_i^\dagger b_i = 1 \quad (51)$$

The constraint will later on be enforced through Lagrange multipliers λ_i , which will add a term of:

$$\int d\lambda \exp \left\{ \int d\tau \left(-i \sum_i \lambda_i (\sum_{\sigma} f_{i\sigma}^\dagger f_{i\sigma} + b_i^\dagger b_i - 1) \right) \right\} \quad (52)$$

to the partition function. This term integrated out, will enforce the constraint, so that we do not have to worry about it any longer.

After having introduced the idea of the slave boson description it will now be applied and the t-J Hamiltonian will be rewritten in terms of the spinon (fermionic) operators $f_{i\sigma}^\dagger/f_{i\sigma}$ and the holon (boson) operators b_i^\dagger/b_i . To achieve this $S_i \cdot S_j$ and $n_i n_j$ have to be rewritten to obtain the t-J Hamiltonian from Eq. 47 in terms of f and b . The number of electrons on site i n_i is just 1 minus the number of holes on that site which can be written as:

$$n_i = 1 - b_i^\dagger b_i \quad (53)$$

For the product of $n_i n_j$ the nearest neighbor holon-holon interaction $b_i^\dagger b_i b_j^\dagger b_j$ will be neglected, since it is small in low doping, i.e. the probability of two holes next to each other is very low, so that it can be neglected.

If one now wants to rewrite $\vec{S}_i \cdot \vec{S}_j$, one first has to take a look at the definition of \vec{S}_i which is given by

$$\vec{S}_i = \frac{1}{2} c_{i\alpha}^\dagger \vec{\sigma}_{\alpha\beta} c_{i\beta} \quad (54)$$

From this definition a straight forward, but slightly tedious calculation then yields

$$\vec{S}_i \cdot \vec{S}_j = -\frac{1}{4} f_{i\alpha}^\dagger f_{j\alpha} f_{j\beta}^\dagger f_{i\beta} - \frac{1}{4} (f_{i\uparrow}^\dagger f_{j\downarrow}^\dagger - f_{i\downarrow}^\dagger f_{j\uparrow}^\dagger) (f_{j\downarrow} f_{i\uparrow} - f_{j\uparrow} f_{i\downarrow}) + \frac{1}{4} f_{i\alpha}^\dagger f_{i\alpha} \quad (55)$$

(see also Ref. [40]). Having now rewritten all terms, we obtain the following Hamiltonian:

$$\begin{aligned}
H = & \sum_i \mu_b b_i^\dagger b_i \\
& - \frac{J}{4} \sum_{\langle i,j \rangle} \sum_{\alpha,\beta=\{\uparrow,\downarrow\}} f_{i\alpha}^\dagger f_{j\alpha} f_{j\beta}^\dagger f_{i\beta} \\
& - \frac{J}{4} \sum_{\langle i,j \rangle} (f_{i\uparrow}^\dagger f_{j\downarrow}^\dagger - f_{i\downarrow}^\dagger f_{j\uparrow}^\dagger) (f_{j\downarrow} f_{i\uparrow} - f_{j\uparrow} f_{i\downarrow}) \\
& - \sum_{i,j} \sum_{\sigma=\{\uparrow,\downarrow\}} t_{ij} f_{i\sigma}^\dagger b_i b_j^\dagger f_{j\sigma}
\end{aligned} \tag{56}$$

Note that some terms, like the constant term and the terms with $f^\dagger f$ and $b^\dagger b$, have been canceled here using the constraint in Eq.51. The term with the $\mu_b b^\dagger b$ is the term one cannot cancel, when using the constraint. The prefactor μ_b here takes a value of $\frac{1}{4}JN$, where $N = 6$ is the number of nearest neighbors.

Looking at this Hamiltonian in Eq. 56 one realizes that most terms are in fourth order in fermionic operators which makes it difficult to obtain physical quantities like the partition function from it. Therefore, in the next section we will use a Hubbard Stratonovich decoupling to simplify the problem.

4.2 Hubbard Stratonovich transformation

Having now obtained the Hamiltonian of the problem we want to simplify it due to the higher order terms in fermionic operators. For this we first write down the partition function, which then will be decoupled using a Hubbard Stratonovich transformation. Using the Hamiltonian from Eq. 56 one can write the partition function of the system as:

$$Z = \int df df^* db db^* d\lambda e^{-\int d\tau L} \tag{57}$$

with

$$\begin{aligned}
L = & \sum_i b_i^\dagger (\partial_\tau + \mu_b) b_i + \sum_{i,\sigma} f_{i\sigma}^\dagger \partial_\tau f_{i\sigma} \\
& - i \sum_i \lambda_i (\sum_\sigma f_{i\sigma}^\dagger f_{i\sigma} + b_i^\dagger b_i - 1) \\
& - \frac{J}{4} \sum_{\langle i,j \rangle} f_{i\alpha}^\dagger f_{j\alpha} f_{j\beta}^\dagger f_{i\beta} \\
& - \frac{J}{4} \sum_{\langle i,j \rangle} (f_{i\uparrow}^\dagger f_{j\downarrow}^\dagger - f_{i\downarrow}^\dagger f_{j\uparrow}^\dagger) (f_{j\downarrow} f_{i\uparrow} - f_{j\uparrow} f_{i\downarrow}) \\
& - \sum_{ij\sigma} t_{ij} f_{i\sigma}^\dagger b_i b_j^\dagger f_{j\sigma}
\end{aligned} \tag{58}$$

where in the second line the constraint of the forbidden double occupation (see Eq. 51) was introduced using a Lagrange multiplier λ_i . This partition function will now be decoupled in three different channels:

- Spinon hopping χ
- Spinon pairing Δ
- Holon spinon interaction F

The decoupling in these channels then yields a more manageable partition function which allows us to better understand the underlying physics. Also the decoupling helps to switch from a monomer description to a dimer description, which makes it possible to compare the results with other research, which tries to explain the different phases of this system in terms of dimers (see e.g. Ref [12]).

4.2.1 Spinon hopping χ

The first decoupling will be performed by introducing a spinon hopping χ , this arises when decoupling the following term:

$$\exp \left(- \int_0^\beta d\tau - \frac{J}{4} \sum_{\langle i,j \rangle} f_{i\alpha}^\dagger f_{j\alpha} f_{j\beta}^\dagger f_{i\beta} \right) \quad (59)$$

This can be straightforwardly decoupled by just using the formula for the Hubbard Stratonovich decoupling, which then yields:

$$\begin{aligned} & \exp \left(- \int_0^\beta d\tau - \frac{J}{4} \sum_{\langle i,j \rangle} f_{i\alpha}^\dagger f_{j\alpha} f_{j\beta}^\dagger f_{i\beta} \right) \\ &= \int D\chi \exp \left(- \int_0^\beta d\tau \frac{J}{4} \sum_{\langle i,j \rangle} (|\chi_{ij}|^2 - \chi_{ij}^* (\sum_\sigma f_{i\sigma}^\dagger f_{j\sigma}) + h.c.) \right) \end{aligned} \quad (60)$$

The decoupling parameter χ_{ij} is here of the form $\sum_\sigma f_{i\sigma}^\dagger f_{j\sigma}$ and describes the hopping of a spinon between two neighboring sites. From the formulation of the decoupling operator one directly sees that $\chi_{ij}\chi_{ji}^\dagger$ which will have important implications in the following sections.

4.2.2 Spinon pairing Δ

Next a spinon pairing will be introduced to decouple the next term, which then using a Hubbard Stratonovich transformation is decoupled as follows:

$$\begin{aligned} & \exp \left(\int_0^\beta d\tau \frac{J}{4} \sum_{\langle i,j \rangle} (f_{i\uparrow}^\dagger f_{j\downarrow}^\dagger - f_{i\downarrow}^\dagger f_{j\uparrow}^\dagger) (f_{j\downarrow} f_{i\uparrow} - f_{j\uparrow} f_{i\downarrow}) \right) \\ &= \int D\Delta \exp \left(- \int_0^\beta d\tau \frac{J}{4} \sum_{\langle i,j \rangle} (|\Delta_{ij}|^2 + \Delta_{ij} (f_{i\uparrow}^\dagger f_{j\downarrow}^\dagger - f_{i\downarrow}^\dagger f_{j\uparrow}^\dagger) + h.c.) \right) \end{aligned} \quad (61)$$

The decoupling field Δ describes the spinon pairing and is of the form $f_{i\uparrow}f_{j\downarrow} - f_{i\downarrow}f_{j\uparrow}$. It is bosonic and describes a spin singlet dimer.

4.2.3 Holon-spinon interaction F

The last term which needs to be decoupled is the holon spinon interaction term. But before doing that it makes sense to symmetrize the term to simplify the calculations later on:

$$\begin{aligned}
& \exp \left(\int_0^\beta d\tau \sum_{ij\sigma} t_{ij} b_i b_j^\dagger f_{i\sigma}^\dagger f_{j\sigma} \right) \\
&= \exp \left(\int_0^\beta d\tau \sum_{ij\sigma} \frac{t_{ij}}{2} (f_{i\sigma}^\dagger b_j^\dagger b_i f_{j\sigma} + f_{j\sigma}^\dagger b_i^\dagger b_j f_{i\sigma}) \right) \\
&= \exp \left(\int_0^\beta d\tau \sum_{ij\sigma} \frac{t_{ij}}{2} [(f_{i\sigma}^\dagger b_j^\dagger + f_{j\sigma}^\dagger b_i^\dagger)(f_{i\sigma} b_j + f_{j\sigma} b_i) - b_i^\dagger b_i - b_j^\dagger b_j + \dots] \right)
\end{aligned} \tag{62}$$

Here the dots refer to holon holon interactions and can be neglected with the same reasoning as before. The first term can now be decoupled which yields:

$$\begin{aligned}
& \exp \left(\int_0^\beta d\tau \sum_{ij\sigma} \frac{t_{ij}}{2} [(f_{i\sigma}^\dagger b_j^\dagger + f_{j\sigma}^\dagger b_i^\dagger)(f_{i\sigma} b_j + f_{j\sigma} b_i)] \right) \\
&= \exp \left(- \int_0^\beta d\tau \sum_{ij\sigma} t_{ij} (\bar{F}_{ij\sigma} F_{ij\sigma} + \frac{1}{\sqrt{2}} \bar{F}_{ij\sigma} (f_{i\sigma} b_j + f_{j\sigma} b_i) + h.c.) \right)
\end{aligned} \tag{63}$$

The Hubbard Stratonovich field F is fermionic and carries both spin and electric charge. The field represents a hole like bound state and one has that

$$F_{ij\sigma} = \frac{1}{\sqrt{2}}(f_{i\sigma} b_j + f_{j\sigma} b_i) \tag{64}$$

which can be identified with a dimer representing a spinon-holon bound state.

After now having performed all three decouplings the terms can be combined and we arrive at the following partition function:

$$Z = \int D b D b^* D f D f^\dagger D \lambda D \chi D \Delta D F e^{\int_0^\beta d\tau L_1} \tag{65}$$

with

$$\begin{aligned}
L_1 = & \sum_i b_i^\dagger (\partial_\tau + \mu_b - i\lambda_i) b_i + \sum_{i,\sigma} f_{i\sigma}^\dagger (\partial_\tau - i\lambda_i) f_{i\sigma} \\
& + \sum_{ij\sigma} t_{ij} (\bar{F}_{ij\sigma} F_{ij\sigma} + \frac{1}{\sqrt{2}} \bar{F}_{ij\sigma} (f_{i\sigma} b_j + f_{j\sigma} b_i) + h.c.) \\
& + \frac{J}{4} \sum_{\langle i,j \rangle} (|\Delta_{ij}|^2 + \Delta_{ij} (f_{i\uparrow}^\dagger f_{j\downarrow}^\dagger - f_{i\downarrow}^\dagger f_{j\uparrow}^\dagger) + h.c.) \\
& + \frac{J}{4} \sum_{\langle i,j \rangle} (|\chi_{ij}|^2 - \chi_{ij}^* (\sum_\sigma f_{i\sigma}^\dagger f_{j\sigma}) + h.c.)
\end{aligned} \tag{66}$$

It is important to note that μ_b now has another value as before due to the terms $b^\dagger b$ in Eq. 62. The exact value is not of great importance here and strongly depends on the choice of t_{ij} , but it is constant as long as t_{ij} is not position dependent (it could depend on the distance between i and j though).

The partition function is neither shorter than before nor does it seem easier at first, but now it allows us to integrate out b and f which means that we switched from a problem formulated through f and b to a problem formulated in terms of the bosonic dimers Δ , fermionic dimer F and spinon hopping χ .

4.3 Different phases

Having now a Lagrangian in terms of F , Δ and χ it makes sense to look at the possible different behaviors of the system, i.e. if there are different phases depending on the different parameters. $\langle \chi \rangle \neq 0$ is the case which corresponds to the resonating valence bond states in the undoped case and using it will lead to the translationally and rotationally invariant states. For $\langle \chi \rangle \neq 0$ we have 4 different phases depending on $\langle \Delta \rangle$ and $\langle b \rangle$. The four phases one has are (see also Fig.10):

- Fermi liquid: $\langle b \rangle \neq 0, \langle \Delta \rangle = 0$
- super conductor: $\langle b \rangle \neq 0, \langle \Delta \rangle \neq 0$
- U(1) fractionalized Fermi liquid: $\langle b \rangle = 0, \langle \Delta \rangle = 0$
- \mathbb{Z}_2 fractionalized Fermi liquid: $\langle b \rangle = 0, \langle \Delta \rangle \neq 0$

While it intuitively makes sense that one has different phases for a different choice of parameters, i.e. setting them 0 or not, it is not directly obvious why a specific phase arises for each choice of parameters. For the Fermi liquid and the superconducting state already a lot explanation has been given by others which will just be shortly teased here, while the fractionalized Fermi liquid states are quite new compared to that and will be looked at in detail in the next sections.

FL	↑	SC
$\langle b \rangle \neq 0$		$\langle b \rangle \neq 0$
$\langle \Delta \rangle = 0$		$\langle \Delta \rangle \neq 0$
U(1)-FL*		\mathbb{Z}_2 -FL*
$\langle b \rangle = 0$		$\langle b \rangle = 0$
$\langle \Delta \rangle = 0$		$\langle \Delta \rangle \neq 0$

Fig. 10: There are four different phases: the Fermi liquid and the superconductor and U(1) and \mathbb{Z}_2 fractionalized Fermi liquid (FL*). Especially, the latter two are of interest in this thesis, since they are not as well understood yet.

If the holons are condensed which corresponds to $\langle b \rangle \neq 0$, one has $c^\dagger = \langle b \rangle f^\dagger$, i.e. $c^\dagger \sim f^\dagger$ and the f fermions describe the full electron, not just its spin. In this case one has a Fermi liquid or a superconducting state:

- The Fermi liquid which arises, when $\langle \Delta \rangle = 0$, is similar to that which arises the heavy-fermion problem (see Ref. [41]). Its properties have been examined by Grilli and Kotliar in Ref. [42].
- The superconducting phase has already been explained in 1987 by Anderson (see Ref [11]) who predicted that the spin singlets of the RVB state become charged superconducting Cooper pairs for large doping. This has later been shown to be correct by Kotliar and Liu [43], who also made predictions on the phases that exist, but without further analyzing them.

4.4 Gauge invariances

Since as described above the Fermi liquid and the superconducting state are already well understood, we will focus now on the state with $\langle b \rangle = 0$ which are the fractionalized Fermi liquid states and will analyze their properties.

One now aims to work with the partition function by integrating out the operators b_i^\dagger/b_i and $f_{i\sigma}^\dagger/f_{i\sigma}$, but this is quite a tedious calculation. To avoid this, we will "guess" the solution of this calculation from gauge invariance and charge conservation arguments. The original Lagrangian in Eq. 58 is U(1) gauge invariant, i.e. it is invariant under transformations of b and f like:

$$f_{i\sigma} \rightarrow f_{i\sigma} e^{i\phi_i} \quad \text{and} \quad (67)$$

$$b_i \rightarrow b_i e^{i\phi_i} \quad (68)$$

These transformations imply how λ has to transform for gauge invariance:

$$\lambda_i \rightarrow \lambda_i + \partial_\tau \phi_i \quad (69)$$

Now taking the definitions of the decoupling fields yields that the effective Lagrangian has to be invariant under transformations like:

$$\Delta_{ij} \rightarrow \Delta_{ij} e^{i(\phi_i + \phi_j)} \quad (70)$$

$$\chi_{ij} \rightarrow \chi_{ij} e^{i(-\phi_i + \phi_j)} \quad (71)$$

$$F_{ij} \rightarrow F_{ij} e^{i(\phi_i + \phi_j)} \quad (72)$$

One sees that the spinon pairing field Δ_{ij} and the fermionic field F_{ij} both come with a gauge charge of two and they both stay the same under the exchange of indices: $F_{ij} = F_{ji}$ and $\Delta_{ij} = \Delta_{ji}$. On the other hand χ_{ij} has no net gauge charge and one also directly sees that $\chi_{ij} \neq \chi_{ji}$. Writing the lowest orders of all terms which fulfill this gauge invariance and electric charge conservation gives:

$$\begin{aligned} L_{eff} = & \sum_{ij} \{ \bar{\chi}_{ij} [\partial_\tau - i(-\lambda_i + \lambda_j)] \chi_{ij} + a_1^\chi |\chi_{ij}|^2 + a_2^\chi |\chi_{ij}|^4 \} + a_3^\chi \sum_{i,j,k,l} \chi_{ij} \chi_{jk} \chi_{kl} \chi_{li} \\ & + \sum_{ij} \{ \bar{\Delta}_{ij} [\partial_\tau - i(\lambda_i + \lambda_j)] \Delta_{ij} + a_1^\Delta |\Delta_{ij}|^2 + a_2^\Delta |\Delta_{ij}|^4 \} + a_3^\Delta \sum_{i,j,k,l} \bar{\Delta}_{ij} \Delta_{jk} \bar{\Delta}_{kl} \Delta_{li} \\ & + \sum_{ij\sigma} \{ \bar{F}_{ij\sigma} [\partial_\tau - i(\lambda_i + \lambda_j)] F_{ij\sigma} + a_1^F \bar{F}_{ij\sigma} F_{ij\sigma} \} \\ & + \sum_{ijkl\sigma} \{ a_1^{F\chi} \bar{F}_{ij\sigma} F_{jk\sigma} \chi_{kl} \chi_{li} + a_2^{F\chi} \bar{F}_{ij\sigma} \bar{\chi}_{jk} F_{kl\sigma} \chi_{li} \\ & + \sum_{ijkl\sigma} \{ a_1^{F\Delta} \bar{F}_{ij\sigma} F_{jk\sigma} \bar{\Delta}_{kl} \Delta_{li} + a_2^{F\Delta} \bar{F}_{ij\sigma} \Delta_{ij} \bar{\Delta}_{kl} F_{kl\sigma} \} \\ & + \sum_{ijkl} \{ a_1^{\Delta\chi} \bar{\Delta}_{ij} \Delta_{jk} \chi_{kl} \chi_{li} + a_2^{\Delta\chi} \bar{\Delta}_{ij} \bar{\chi}_{jk} \Delta_{kl} \chi_{li} + \dots \end{aligned} \quad (73)$$

where the coefficients $a_{1/2}^\square$ are real. The terms not written out are symmetry related terms and terms that encircle more than one plaquette at a time. The λ s have to look like this due to the gauge transformation of λ which was given in Eq. 69.

While most of these terms can be explained with the gauge invariance condition, for the time dependent terms a bit more reasoning has to be done:

To understand how the time derivative terms arise one can take a look at the self interaction diagrams of Δ and F . One can show that in the first order the term is proportional to $i\omega_k$.

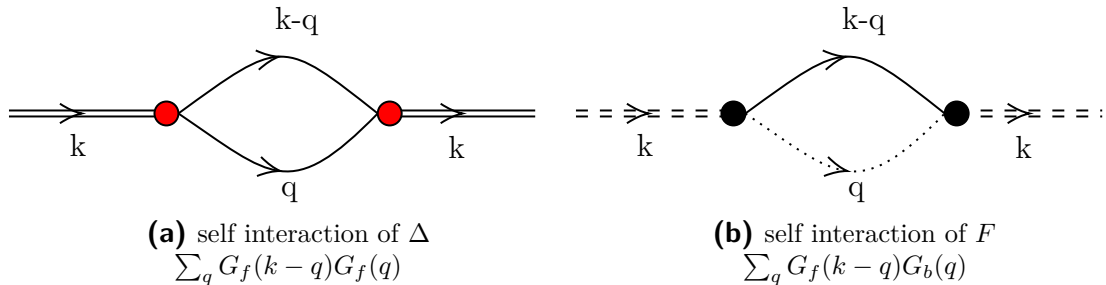


Fig. 11: One loop order terms for $|\Delta|^2$ and $|F|^2$. The diagram was drawn using: a line for f , a dotted line for b , a double dashed line for F and a double line for Δ .

When looking on the first order and therefore one loop interaction of $|\Delta|^2$ or $|F|^2$ as displayed in Fig. 11, one is looking at:

$$\sum_q G_f(k-q)G_f(q) \quad \text{for the } |\Delta|^2 \text{ term and} \quad (74)$$

$$\sum_q G_f(k-q)G_b(q) \quad \text{for the } |F|^2 \text{ term.} \quad (75)$$

Since one has:

$$G_f(\vec{i}, \omega) = \frac{-i}{\lambda_i - i\omega} \quad \text{and} \quad (76)$$

$$G_b(\vec{i}, \omega) = \frac{-i}{i\mu_b + \lambda_i - i\omega} \quad (77)$$

one can calculate and simplify this terms by Taylor expanding for small ω . The terms in Eq. 74 and Eq. 75 are then proportional to $i\omega$. Hence, the first order time derivative.

Also due to gauge invariance also terms containing an odd number of χ (like χ^3) are theoretically allowed in Eq. 73, but we restrict ourselves to the square lattice and therefore end up only with terms encircling a full plaquette.

One also has to note that there is no forth order term in F, which is again due to the fact that then we have a term of the forth order in b, which is negligible. Intuitively this can be seen through the fact that we are close to half filling so the probability of two holes on the same plaquette is low.

4.5 Saddle point

The Lagrangian in Eq. 73 still looks quite complicated, but now we can actually draw some conclusions from it. First, we will look at the saddle point solution for $\chi = \chi_0$ with $\chi_0 \in \mathbb{R}$. Then the problem simplifies a lot and depending on the choice of $\langle \Delta \rangle$ one then obtains a $U(1)$ or \mathbb{Z}_2 fractionalized Fermi liquid.

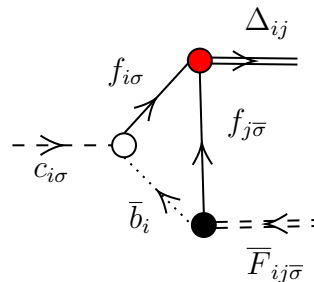


Fig. 12: The electron operator $c_{i\sigma}$ can be written as the diagram above, which makes it possible to switch between the dimer description in terms of the dimers Δ_{ij} and $F_{ij\sigma}$ and the electron operator $c_{i\sigma}$.

The description in terms of dimers is nice to draw conclusions about the physical behavior of the system, but in the end we would like to transfer the description back to a description in terms of the electron operator, since the electric properties can be compared with experiments. In the saddle point approximation we can express the electron field as (see Fig.12):

$$c_{i\sigma} \sim \sum_j \bar{F}_{ij\bar{\sigma}} \Delta_{ij} \quad (78)$$

where the bar over the σ indicates that it is the opposite spin of σ .

4.5.1 U(1) fractionalized Fermi liquid

For $\langle \Delta \rangle = 0$ we have a so called "strange metal". It can be described by a U(1) fractionalized Fermi liquid. As we look at the problem at the saddle point $\langle \chi \rangle = \chi_0$ the terms which capture the interactions in Eq. 73 are:

$$\begin{aligned} & a_3^\Delta \sum_{i,j,k,l} \bar{\Delta}_{ij} \Delta_{jk} \bar{\Delta}_{kl} \Delta_{li} \\ & + a_1^{F\Delta} \sum_{ijkl\sigma} \bar{F}_{ij\sigma} F_{jk\sigma} \bar{\Delta}_{kl} \Delta_{li} \\ & + a_2^{F\Delta} \sum_{ijkl\sigma} \bar{F}_{ij\sigma} \Delta_{ij} \bar{\Delta}_{kl} F_{kl\sigma} \end{aligned} \quad (79)$$

These terms are displayed in Fig. 13 and correspond to switching a fermionic and a bosonic dimer or turning a plaquette with either two bosonic dimers or one bosonic and one fermionic dimer. These terms are exactly the same as the Hamiltonian which has been derived in Ref. [12](see also Sec. 2.2). This is further evidence that the method used is self-consistent. It is important to note, that there are no terms quadratic in F or Δ from the terms $\sim a^{\Delta\chi}$ and $\sim a^{F\chi}$ in Eq. 73 due to the hardcore constraint. The hardcore constraint is ensured in this model through the constraint on the particle number (Lagrange multiplier).

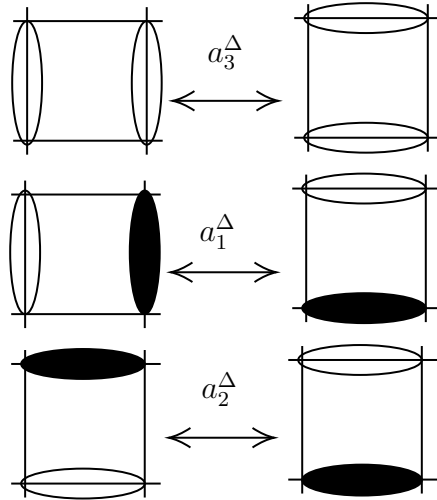


Fig. 13: The important interaction on a plaquette in a U(1) fractionalized Fermi liquid (see also Eq. 79). The bosonic dimer Δ is represented through an empty oval, while the fermionic dimer is shown through a black filled oval.

The fact that Eq. 79 and the Hamiltonian in Ref. [12] are the same also implies that all the findings about the U(1) fractionalized Fermi liquid state in other papers are valid in this description, too. One has that the creation operator of a bosonic spin singlet is given by

$$\Delta_{j,\eta}^\dagger = \frac{1}{\sqrt{2}}(f_{j\uparrow}^\dagger f_{j+\eta\downarrow}^\dagger - f_{j\downarrow}^\dagger f_{j+\eta\uparrow}^\dagger) \quad (80)$$

and that F creates a fermionic dimer representing a spinon holon bound state with:

$$F_{j,\eta,\sigma}^\dagger = \frac{1}{\sqrt{2}}(f_{j\sigma}^\dagger b_{j+\eta}^\dagger + f_{j+\eta\sigma}^\dagger b_j^\dagger) \quad (81)$$

Also it has been shown in Ref [44] that this state has a small sharp electronic Fermi surface, which has also been found in experiments on cuprates. Those small Fermi surfaces appear close to the momenta $k = (\pm\pi/2, \pm\pi/2)$ and in this case the Fermi volume is proportional to the doping away from half filling, which is different to the usual Fermi liquid, where the Fermi surface is proportional to $1 + p$, where p is the doping.

In this theory one also has sharp quasiparticle excitations. From Eq. 78 we have that the electronic operator is a convolution of F and Δ , so this is not very intuitive, but this is due to the hardcore constraint which keeps Δ and F local. The electron spectral function shows Fermi arc like features due to the anisotropically distributed electronic quasi-particle weight.

4.5.2 \mathbb{Z}_2 fractionalized Fermi liquid

For $\langle\Delta\rangle \neq 0$ we have a so called "pseudogap" state. In this case though it is a \mathbb{Z}_2 fractionalized Fermi liquid. In this case one can conclude from Eq 78 that the

electronic operator can be written as:

$$c_{i\sigma} \sim \sum_j \bar{F}_{ij\bar{\sigma}} \quad (82)$$

this also implies that the electronic Fermi surface coincides with the Fermi surface of the fermionic operator F , which is fixed by the hole density (depends on the operator b). This implies that the Fermi surface is small and also explains the change in the Luttinger relation: instead of being proportional to $1 + p$, where p is the doping, as it would be for a Fermi liquid, the Luttinger count is proportional to F and therefore directly proportional to the doping p .

Depending on the sign of the coefficient a_3^Δ in Eq. 73 one can choose the following translationally invariant saddle point solutions for Δ :

- for $a_3^\Delta < 0$: $\langle \Delta_{i,x} \rangle = \langle \Delta_{i,y} \rangle = \Delta$
- for $a_3^\Delta > 0$: $\langle \Delta_{i,x} \rangle = \Delta$ and $\langle \Delta_{i,y} \rangle = i\Delta$

We will focus on the first point here and since both cases are quite similar, just remark on the second point in the end. The effective Hamiltonian is given by:

$$H_{\mathbb{Z}_2} = -t_1 \sum_{j,\sigma} F_{j+y,x,\sigma}^\dagger F_{j,x,\sigma} - t_2 \sum_{j,\sigma} F_{j,y,\sigma}^\dagger F_{j,x,\sigma} - t_3 \sum_{j,\sigma} F_{j+y,y,\sigma}^\dagger F_{j,x,\sigma} + \dots \quad (83)$$

where $t_1 = -a_2^{F\Delta} |\Delta|^2 - a_2^{F\chi} |\chi|^2$ and $t_2 = -a_1^{F\Delta} |\Delta|^2 - a_1^{F\chi} |\chi|^2$. As always the dots represent the symmetry related terms. These terms are displayed in Fig. 14. Note that t_3 arises from terms comprising a process of two (or even more) plaquettes, so it comes from higher order terms, which were not explicitly written down in L_{eff} (Eq. 73). One could argue that those processes happen a lot less than the processes on a single plaquette, but including this term makes it better comparable to other findings (e.g. in Ref. [12] terms comprising two plaquettes have been treated).

Rewrite electron operator (see Eq.78) as

$$c_{k\sigma} \sim \Delta \sum_\eta F_{-k,\eta,\bar{\sigma}}^\dagger (1 + e^{ik\eta}) \quad (84)$$

with the help of a Fourier transformation.

For $a_3^\Delta > 0$ the saddle point is at $\Delta_{i,x} = \Delta$ and $\Delta_{i,y} = i\Delta$. This leaves the terms in Eq. 83 with t_1 and t_2 unchanged. The term with t_3 changes the sign in this case.

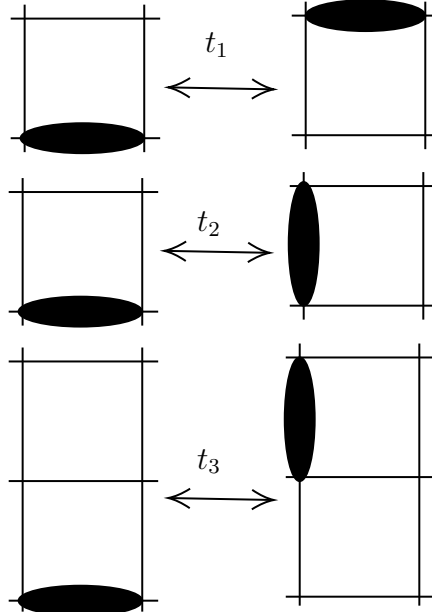


Fig. 14: The important interactions on a plaquette in a \mathbb{Z}_2 fractionalized Fermi liquid (see also Eq. 83).

4.5.3 Notes on π - flux state

Up to now we only discussed the simplest choice for χ_{ij} with $\langle \chi_{ij} \rangle = \chi_0$, but there is also another choice which has been of high scientific interest (see e.g. Ref. [19] Chapter VI or Ref. [45]): the π flux state, which corresponds to the following choice of χ_{ij} :

$$\langle \chi_{ij} \rangle = \chi_0 \exp \left\{ i \frac{\pi}{4} (-1)^{i_x + j_y} \right\} \quad (85)$$

This would change all the calculations performed before, but that it does not change the underlying physics of the system will be shown here. One can make plausible that the change of the choice of χ does not change much by looking at the gauge charge of the F fermions: The F fermions have a gauge charge of 2 therefore they pick up an Aharonov Bohm phase (see Ref. [46]) of 2π when encircling a plaquette. In a more explicit manner one can show that not much changes with this choice of χ by looking at the following terms in the Lagrangian:

$$\sum_{ijkl} \left(a_1^{F\chi} \bar{F}_{ij\sigma} F_{jk\sigma} \chi_{kl} \chi_{li} + a_2^{F\chi} \bar{F}_{ij\sigma} \bar{\chi}_{jk} F_{kl} \chi_{li} \right) \quad (86)$$

One can directly note that the second term is for the π flux state and the constant χ , since both χ and $\bar{\chi}$ pick up phases with opposite signs which cancel each other. One has to have $\chi_{ij} = \bar{\chi}_{ji}$ due to the gauge transformation χ has. Paired with the fact that when encircling a plaquette the phases induced by χ all have the same sign this explains why the term $\sim a_2^{F\chi}$ stays the same for the different choices of χ . One is usually interested in energy dispersion in terms of momenta. Therefore, we will Fourier transform the terms from above and at the same time plug in the χ s.

For the π flux state it is easier to work with a bigger unit cell, since the sign of the phase depends on the sites of the dimer i and j having even or odd indices. The new unit cell is displayed in Fig. 15 and solves this problem.

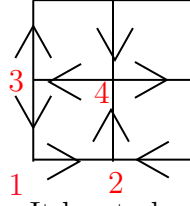


Fig. 15: Unit cell in the π flux state. It has to be bigger than in the case $\chi = \chi_0$ since the sign of the phase attributed to each dimer depends on the sites having even or odd indices. The arrows here indicate the direction of χ_s that are associated with a phase of $+\pi/4$, e.g. $\chi_{1,x}$ gives a phase of $+\pi/4$ while $\chi_{1,y}$ gives a phase of $-\pi/4$. It is important to note that in the π flux state one has $\chi_{ij} = \bar{\chi}_{ji}$.

From the position dependent form with the new unit cell we will switch to the momentum description by using a Fourier transform. This then means that the terms of the Lagrangian will be rewritten as:

$$(\bar{F}_{1,x}, \bar{F}_{1,y}, \bar{F}_{2,x}, \bar{F}_{2,y}, \bar{F}_{3,x}, \bar{F}_{3,y}, \bar{F}_{4,x}, \bar{F}_{4,y}) M \begin{pmatrix} F_{1,x} \\ F_{1,y} \\ F_{2,x} \\ F_{2,y} \\ F_{3,x} \\ F_{3,y} \\ F_{4,x} \\ F_{4,y} \end{pmatrix} \quad (87)$$

As mentioned above, for the comparison it is sufficient to look only at the term proportional to $a_1^{F\chi}$, since it is the only term which changes between both state. For this term we obtain M to be:

$$M = a_1^{F\chi} e^{i\frac{\pi}{2}} \begin{pmatrix} 0 & 1 & 0 & -1 & 0 & e^{ik_y} & 0 & -e^{ik_y} \\ -1 & 0 & -e^{ik_x} & 0 & 1 & 0 & e^{ik_x} & 0 \\ 0 & e^{-ik_x} & 0 & -1 & 0 & e^{ik_y - ik_x} & 0 & -e^{ik_y} \\ 1 & 0 & 1 & 0 & -1 & 0 & -1 & 0 \\ 0 & -1 & 0 & 1 & 0 & -1 & 0 & 1 \\ -e^{-ik_y} & 0 & -e^{ik_x - ik_y} & 0 & 1 & 0 & e^{ik_x} & 0 \\ 0 & -e^{-ik_x} & 0 & 1 & 0 & -e^{-ik_x} & 0 & 1 \\ e^{-ik_y} & 0 & e^{-ik_y} & 0 & -1 & 0 & -1 & 0 \end{pmatrix} \quad (88)$$

All the additions to the state with $\chi = \chi_0$ have been marked in red. If one now looks at the ground state energy, which corresponds to the lowest eigenvalue of the matrix M, one can see that it is the same for both cases (see Fig. 16). These plots only differ at an order of 10^{-15} which is due to computational rounding.

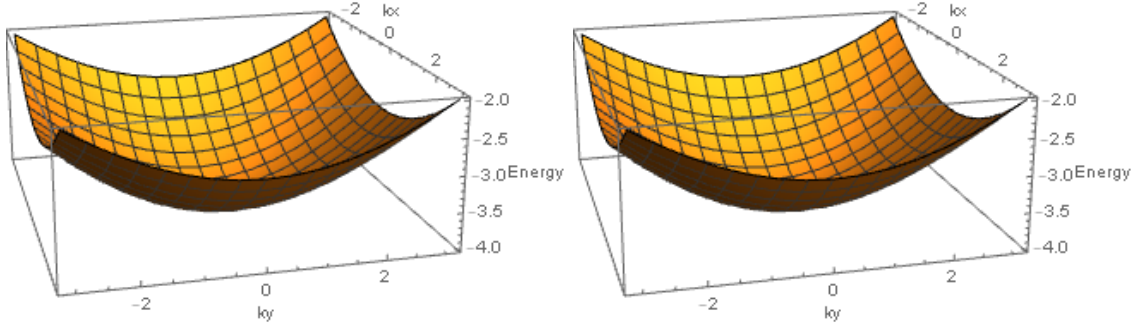
(a) π flux state(b) χ const

Fig. 16: For the different choices of χ the ground state is the same. The plots differ only at an order of up to 10^{-15} which is probably only due computational rounding.

So one can conclude that the dispersion of the F fermions for the π flux state is indeed the same as for the case $\chi = \chi_0$.

4.6 Gauge fluctuations

Having now looked at the mean field solutions it makes sense to allow now small deviations from the saddle point solution for χ . For this phase fluctuations for χ on nearest neighbor bonds will be allowed. Here it is crucial to remember: $\chi_{ij} = \bar{\chi}_{ji}$. From this we will derive a theory for F and Δ coupled to a U(1) gauge field A . This gauge field will be introduced by allowing the following fluctuations for χ :

$$\chi_{i\eta} = \chi_0 e^{iA_i^\eta} \quad (89)$$

where A_i^η parametrizes the phase fluctuation of $\chi_{i,\eta}$ on the bond starting from lattice site i in direction η , which can be x or y on the square lattice. This will now be used to simplify the Lagrangian in Eq. 73. The most important terms to consider are the term $\sim a_3^\chi$ and the terms $\sim a_{1,2}^{F\chi}$ and $\sim a_{1,2}^{\Delta\chi}$.

The term $\sim a_3^\chi$ then takes the form:

$$a_3^\chi \chi^4 \sum_j \exp(A_j^x + A_{j+x}^y - A_{j+y}^x - A_j^y) + \text{h.c.} \quad (90)$$

From this now takes the continuum limit such that $A_j^x - A_{j+y}^x$ becomes $\partial_y A^x$ and the sum over all lattice points \sum_j becomes an integral $\int d^2x$. This leads to a Maxwell term for a compact U(1) gauge theory in 2+1 dimensions:

$$2a_3^\chi \chi^4 \int d^2x \cos(\partial_x A^y - \partial_y A^x) \quad (91)$$

The next step is to look at the interactions between the gauge field and F/Δ are the terms $\sim a_{1,2}^{F\chi}$ and $\sim a_{1,2}^{\Delta\chi}$:

$$\begin{aligned} & a_1^{F\chi} \chi^2 \sum_{i\sigma} \bar{F}_{iy\sigma} F_{ix\sigma} e^{i(A_{i+x}^y - A_{i+y}^x)} + a_2^{F\chi} \chi^2 \sum_{i\sigma} \bar{F}_{i,x\sigma} F_{i+y,x\sigma} e^{i(A_{i+x}^y - A_i^y)} + \dots \\ & + a_1^{\Delta\chi} \chi^2 \sum_i \bar{\Delta}_{iy} \Delta_{ix} e^{i(A_{i+x}^y - A_{i+y}^x)} + a_2^{\Delta\chi} \chi^2 \sum_i \bar{\Delta}_{i,x} \Delta_{i+y,x} e^{i(-A_{i+x}^y - A_i^y)} + \dots \end{aligned} \quad (92)$$

where the dots indicate symmetry related terms. Since the terms for Δ and F have completely the same form it is enough to do the calculation once and then deduce the result for the other variable (or the other spin in the case of F). The term will now be rewritten by taking the continuum limit, e.g. rewriting

$$F_{i+\eta,\eta'} = (1 + \partial_\eta + \frac{1}{2}\partial_\eta^2) F_{i,\eta'} \quad (93)$$

The spin index has been omitted, since there is no term containing different spins and will be added again in the final result. Then the first line of Eq. 92 can be rewritten as

$$(F_{ix}, F_{iy}) \begin{pmatrix} m_{xx} & m_{xy} \\ m_{xy} & m_{yy} \end{pmatrix} \begin{pmatrix} F_{ix} \\ F_{iy} \end{pmatrix} \quad (94)$$

with

$$m_{xx} = a_2^{F\chi} \chi^2 \left((1 - \partial_y + \frac{1}{2}\partial_y^2) e^{i(A_i^y + A_{i+x}^y)} + e^{-i(A_i^y + A_{i+x}^y)} (1 + \partial_y + \frac{1}{2}\partial_y^2) \right) \quad (95)$$

$$\begin{aligned} m_{xy} = & a_1^{F\chi} \chi^2 \left(e^{i(-A_i^y - A_{i+y}^x)} (1 + \partial_x + \frac{1}{2}\partial_x^2) + (1 - \partial_y + \frac{1}{2}\partial_y^2) e^{i(A_i^x + A_{i+x}^y)} \right. \\ & \left. + e^{i(A_{i+y}^x - A_{i+x}^y)} + (1 - \partial_y + \frac{1}{2}\partial_y^2) e^{i(-A_i^x + A_i^y)} (1 + \partial_x + \frac{1}{2}\partial_x^2) \right) \end{aligned} \quad (96)$$

To obtain m_{yx} and m_{yy} one just simply has to exchange all x and y in the equations above. Next one diagonalizes M which leads to the eigenvalues:

$$\lambda_{1,2} = \frac{m_{xx} + m_{yy}}{2} \pm \sqrt{\left(\frac{m_{xx} - m_{yy}}{2}\right)^2 + m_{yx}m_{xy}} \quad (97)$$

The lower eigenvalue corresponds to the ground state energy. Tayloring the exponentials and carefully rewriting everything leads to the following term:

$$(a_2^{F\chi} - a_1^{F\chi}) \left(4 + \frac{1}{2}(\nabla - 2i\vec{A})^2 \right) \quad (98)$$

where $\vec{A} = (A^x, A^y)^T$. This term is proportional to $(\nabla - 2iA)^2$. So, this leads to a complete Lagrangian of :

$$\begin{aligned} L = & \sum_\sigma \bar{F}_\sigma [(\partial_\tau - i2A^\tau) - (\nabla - i2\vec{A})^2 - \mu_F] F_\sigma \\ & + \bar{\Delta} [(\partial_\tau - i2A^\tau) - (\nabla - i2\vec{A})^2 + a_1^\Delta] \Delta \\ & + a_2^\Delta |\Delta|^4 + S_{Maxwell}[A^\mu] \end{aligned} \quad (99)$$

The time component of the gauge field was introduced by defining it as the Lagrange multiplier term: $A_i^T \equiv \lambda_i$.

Looking at this Lagrangian we can again see the different types of fractionalized Fermi liquid occurring here:

- For $\langle \Delta \rangle = 0$ one obtains a U(1) fractionalized Fermi liquid, where the F fermions are coupled to a U(1) gauge field \vec{A} .
- If the spinon pair field gets condensed by setting $a_1^\Delta < 0$, one has spontaneous symmetry breaking, which results in the U(1) field being gapped out via the Higgs mechanism (see Ref. [47]). This then leads to a \mathbb{Z}_2 fractionalized Fermi liquid.

5 Conclusion and outlook

In this thesis two different approaches have been used to get a better understanding of the pseudogap state occurring in high T_C superconductors and materials like twisted bilayer graphene. While the first part of this thesis focused on a very specific property of twisted bilayer graphene, the second part more focused on getting a better understanding of the different phases occurring in hole-doped Mott insulators in general.

In the first half of this thesis we started from a dimer description of a triangular lattice by introducing bosonic and fermionic dimer operators. The physics of those dimer can be described by the RK Hamiltonian with added boson-fermion interactions. Looking at the exactly solvable point for this Hamiltonian and adding some small perturbation my predecessor Brin Verheijden was able to find the dispersion relation for the ground state.

Starting from there we took a look at the band structure of this ground state at the pseudogaps when inducing a magnetic field. By introducing a magnetic field through a Peierls substitution we looked at the eigenvalue equation for the problem. The eigenvalue equation is only solvable for certain fractional choices of the magnetic field, but the results can be extended by analytic continuation. The band structure was found and plotted by solving the eigenvalue equation using some constraints. This led us to a Hofstadter butterfly like plot giving predictions for experiments.

In the second half the slave boson method was applied to get a better understanding of the different phases that occur for the t-J model on the square lattice. To achieve this the slave boson version of the t-J Hamiltonian was Hubbard Stratonovich decoupled in three different channels: the spinon hopping, the spinon pairing and the holon spinon interaction. The latter was decoupled using a fermionic HS field on the lattice bonds to account for spinon-holon bound states. This model omits four different phases:

- Fermi liquid
- superconductor
- U(1) fractionalized Fermi liquid
- \mathbb{Z}_2 fractionalized Fermi liquid

The latter two states have been further investigated, since they might be able to explain the behavior of the pseudogap metal phase observed in experiments. For both of these phases the results at the saddle point coincide with other findings for

the dimer model. It is noteworthy that the spinon pairing operator and the holon spinon interaction operator take the same role as the bosonic and fermionic dimer respectively. It has also been looked at the Lagrangian for small deviations from the saddle point, for which one again recovers the two different types of fractionalized Fermi liquid: one with $U(1)$ gauge invariance and one with \mathbb{Z}_2 gauge invariance. Our approach can be used as a starting point to study interesting quantum phase transitions between ordinary Fermi liquids and fractionalized Fermi liquids. Moreover, a generalization to $SU(2)$ slave-boson descriptions is possible as well and might provide insight into recent $SU(2)$ gauge theories for cuprates (see Ref. [48]).

Bibliography

- [1] Shoji Tanaka. High-temperature superconductivity: History and outlook. *JSAP International*, 2001.
- [2] Fatemi V. Fang S. et al. Cao, Y. Unconventional superconductivity in magic-angle graphene superlattices. *Nature*, page 43–50, March 2018.
- [3] Louis Taillefer. Scattering and pairing in cuprate superconductors. *Annual Review of Condensed Matter Physics*, 1, Mar 2010.
- [4] Elbio Dagotto. Correlated electrons in high-temperature superconductors. *Rev. Mod. Phys.*, 66:763–840, Jul 1994.
- [5] Masao Ogata and Hidetoshi Fukuyama. The t–J model for the oxide high-Tc superconductors. *Reports on Progress in Physics*, 71(3):036501, feb 2008.
- [6] Thomas Maier, Mark Jarrell, Thomas Pruschke, and Matthias H. Hettler. Quantum cluster theories. *Rev. Mod. Phys.*, 77:1027–1080, Oct 2005.
- [7] G. Kotliar, S. Y. Savrasov, K. Haule, et al. Electronic structure calculations with dynamical mean-field theory. *Rev. Mod. Phys.*, 78:865–951, Aug 2006.
- [8] Nikolay Prokofév and Boris Svistunov. Bold diagrammatic Monte Carlo technique: When the sign problem is welcome. *Phys. Rev. Lett.*, 99:250201, Dec 2007.
- [9] Alexandru Macridin, M. Jarrell, Thomas Maier, et al. Pseudogap and antiferromagnetic correlations in the Hubbard model. *Phys. Rev. Lett.*, 97:036401, Jul 2006.
- [10] M. Civelli, M. Capone, A. Georges, et al. Nodal-antinodal dichotomy and the two gaps of a superconducting doped Mott insulator. *Phys. Rev. Lett.*, 100:046402, Jan 2008.
- [11] P. W. Anderson. The resonating valence bond state in La_2CuO_4 and superconductivity. *Science*, 235(4793):1196–1198, 1987.
- [12] Matthias Punk, Andrea Allais, and Subir Sachdev. Quantum dimer model for the pseudogap metal. *Proceedings of the National Academy of Sciences*, 112(31):9552–9557, 2015.

-
- [13] Andrea Damascelli, Zahid Hussain, and Zhi-Xun Shen. Angle-resolved photoemission studies of the cuprate superconductors. *Rev. Mod. Phys.*, 75:473–541, Apr 2003.
- [14] H.-B. Yang, J. D. Rameau, Z.-H. Pan, et al. Reconstructed Fermi surface of underdoped $\text{Bi}_2\text{Sr}_2\text{CaCu}_2\text{O}_{8+\delta}$ cuprate superconductors. *Phys. Rev. Lett.*, 107:047003, Jul 2011.
- [15] Kyle M. Shen, F. Ronning, D. H. Lu, et al. Nodal quasiparticles and antinodal charge ordering in $\text{Ca}_{2-x}\text{Na}_x\text{CuO}_2\text{Cl}_2$. *Science*, 307(5711):901–904, 2005.
- [16] M. Platié, J. D. F. Mottershead, I. S. Elfimov, et al. Fermi surface and quasiparticle excitations of overdoped $\text{Tl}_2\text{Ba}_2\text{CuO}_{6+\delta}$. *Phys. Rev. Lett.*, 95:077001, Aug 2005.
- [17] S E Barnes. New method for the Anderson model. *Journal of Physics F: Metal Physics*, 6(7):1375–1383, Jul 1976.
- [18] Gabriel Kotliar and Jialin Liu. Superexchange mechanism and d-wave superconductivity. *Phys. Rev. B*, 38:5142–5145, Sep 1988.
- [19] Patrick A. Lee, Naoto Nagaosa, and Xiao-Gang Wen. Doping a Mott insulator: Physics of high-temperature superconductivity. *Rev. Mod. Phys.*, 78:17–85, Jan 2006.
- [20] Seyed Iman Mirzaei, Damien Stricker, Jason N. Hancock, et al. Spectroscopic evidence for Fermi liquid-like energy and temperature dependence of the relaxation rate in the pseudogap phase of the cuprates. *Proceedings of the National Academy of Sciences of the United States of America*, 110(15):5774–5778, April 2013.
- [21] P. Béran, D. Poilblanc, and R.B. Laughlin. Evidence for composite nature of quasiparticles in the 2d t-J model. *Nuclear Physics B*, 473(3):707 – 720, 1996.
- [22] Tiago C. Ribeiro and Xiao-Gang Wen. New mean-field theory of the $tt't''J$ model applied to high- T_c superconductors. *Phys. Rev. Lett.*, 95:057001, Jul 2005.
- [23] Tai-Kai Ng. Spinon-holon binding in $t-J$ model. *Phys. Rev. B*, 71:172509, May 2005.
- [24] Dale R. Harshman and Anthony T. Fiory. High- T_C superconductivity originating from interlayer coulomb coupling in gate-charged twisted bilayer graphene Moiré superlattices. *Journal of Superconductivity and Novel Magnetism*, 33:367–378, Feb 2020.
- [25] Brin Verheijden, Yuhao Zhao, and Matthias Punk. Solvable lattice models for metals with \mathbb{Z}_2 topological order. *SciPost Phys.*, 7:74, 2019.

- [26] Douglas R. Hofstadter. Energy levels and wave functions of Bloch electrons in rational and irrational magnetic fields. *Phys. Rev. B*, 14:2239–2249, Sep 1976.
- [27] J. Hubbard. Electron correlations in narrow energy bands. *Proceedings of the Royal Society of London. Series A, Mathematical and Physical Sciences*, 276:238–257, 1963.
- [28] Jozef Spalek. t-J model then and now: a personal perspective from the pioneering times. *Acta Physica Polonica A*, 111:409, Apr 2007.
- [29] P.W. Anderson. Resonating valence bonds: A new kind of insulator? *Materials Research Bulletin*, 8(2):153 – 160, 1973.
- [30] Brin Verheijden. Two-species quantum dimer models on the triangular lattice. Master’s thesis, Ludwig-Maximilians-Universität, Jan 2019.
- [31] Daniel S. Rokhsar and Steven A. Kivelson. Superconductivity and the quantum hard-core dimer gas. *Phys. Rev. Lett.*, 61:2376–2379, Nov 1988.
- [32] R. Moessner and K. S. Raman. Quantum dimer models. *arXiv e-prints*, page arXiv:0809.3051, Sep 2008.
- [33] Isabelle Dumé (P Jarillo-Herrero). Ferromagnetism appears in twisted bilayer graphene. <https://physicsworld.com/a/ferromagnetism-appears-in-twisted-bilayer-graphene/>, Jul 2019.
- [34] R. Peierls. Zur Theorie des Diamagnetismus von Leitungselektronen. *Zeitschrift für Physik*, 80(11-12):763–791, November 1933.
- [35] Dieter Langbein. The tight-binding and the nearly-free-electron approach to lattice electrons in external magnetic fields. *Phys. Rev.*, 180:633–648, Apr 1969.
- [36] F. H. Claro and G. H. Wannier. Magnetic subband structure of electrons in hexagonal lattices. *Phys. Rev. B*, 19:6068–6074, Jun 1979.
- [37] Rammal, R. Landau level spectrum of Bloch electrons in a honeycomb lattice. *J. Phys. France*, 46(8):1345–1354, 1985.
- [38] F. Yilmaz and M. Ö. Oktel. Hofstadter butterfly evolution in the space of two-dimensional Bravais lattices. *Phys. Rev. A*, 95:063628, Jun 2017.
- [39] Piers Coleman. New approach to the mixed-valence problem. *Phys. Rev. B*, 29:3035–3044, Mar 1984.
- [40] G. Baskaran, Z. Zou, and P.W. Anderson. The resonating valence bond state and high-Tc superconductivity — a mean field theory. *Solid State Communications*, 63:973–976, Mar 1987.

-
- [41] Patrick A. Lee and Naoto Nagaosa. Gauge theory of the normal state of high- T_c superconductors. *Phys. Rev. B*, 46:5621–5639, Sep 1992.
- [42] Marco Grilli and Gabriel Kotliar. Fermi-liquid parameters and superconducting instabilities of a generalized t-J model. *Phys. Rev. Lett.*, 64:1170–1173, Mar 1990.
- [43] Gabriel Kotliar and Jialin Liu. Superexchange mechanism and d-wave superconductivity. *Phys. Rev. B*, 38:5142–5145, Sep 1988.
- [44] Johannes Feldmeier, Sebastian Huber, and Matthias Punk. Exact solution of a two-species quantum dimer model for pseudogap metals. *Phys. Rev. Lett.*, 120:187001, May 2018.
- [45] Ian Affleck and J. Brad Marston. Large-n limit of the Heisenberg-Hubbard model: Implications for high- T_c superconductors. *Phys. Rev. B*, 37:3774–3777, Mar 1988.
- [46] Y. Aharonov and D. Bohm. Significance of electromagnetic potentials in the quantum theory. *Phys. Rev.*, 115:485–491, Aug 1959.
- [47] P. W. Anderson. Plasmons, gauge invariance, and mass. *Phys. Rev.*, 130:439–442, Apr 1963.
- [48] Subir Sachdev, Harley D. Scammell, Mathias S. Scheurer, and Grigory Tarnopolsky. Gauge theory for the cuprates near optimal doping. *Phys. Rev. B*, 99:054516, Feb 2019.

Statement of authorship

I hereby declare that I am the sole author of this master thesis and that I have not used any sources other than those listed in the bibliography and identified as references. I further declare that I have not submitted this thesis at any other institution in order to obtain a degree.

München, 06.08.2020

Julia Brunkert